CIR MORPHOLOGY, TURBULENCE, DISCONTINUITIES, AND ENERGETIC PARTICLES

Report of Working Group 2

N. U. CROOKER[1] AND J. T. GOSLING[2]
CO-CHAIRS

V. BOTHMER[3], R. J. FORSYTH[4], P. R. GAZIS[5], A. HEWISH[6], T. S. HORBURY[4,7], D. S. INTRILIGATOR[8], J. R. JOKIPII[9], J. KÓTA[9], A. J. LAZARUS[10], M. A. LEE[11], E. LUCEK[4], E. MARSCH[12], A. POSNER[3], I. G. RICHARDSON[13], E. C. ROELOF[14], J. M. SCHMIDT[4], G. L. SISCOE[1], B. T. TSURUTANI[15], AND R. F. WIMMER-SCHWEINGRUBER[16]
PARTICIPANTS

[1] *Center for Space Physics, Boston University, Boston, Massachusetts, USA*
[2] *Los Alamos National Laboratory, Los Alamos, New Mexico, USA*
[3] *Extraterrestriche Physik, University of Kiel, Kiel, Germany*
[4] *Imperial College, London, UK*
[5] *San Jose State University Foundation, NASA Ames Research Center, Moffett Field, California, USA*
[6] *Cavendish Laboratory, Cambridge, UK*
[7] *now at Queen Mary and Westfield College, London*
[8] *Carmel Research Center, Santa Monica, California, USA*
[9] *Lunar Planetary Laboratory, University of Arizona, Tucson, Arizona, USA*
[10] *Center for Space Research, Massachusetts Institute of Technology, Cambridge, Mass., USA*
[11] *University of New Hampshire, Durham, New Hampshire, USA*
[12] *Max-Planck-Institut für Aeronomie, Katlenburg-Lindau, Germany*
[13] *NASA Goddard Space Flight Center, Greenbelt, Maryland, USA (also at Department of Astronomy, University of Maryland, College Park)*
[14] *Applied Physics Laboratory, Johns Hopkins University, Laurel, Maryland, USA*
[15] *Jet Propulsion Laboratory, California Institute of Technology, Pasadena, California, USA*
[16] *Physikalisches Institut der Universität Bern, Bern, Switzerland*

Received: 31 March, 1999; Accepted: 22 May, 1999

Abstract. Corotating interaction regions (CIRs) in the middle heliosphere have distinct morphological features and associated patterns of turbulence and energetic particles. This report summarizes current understanding of those features and patterns, discusses how they can vary from case to case and with distance from the Sun and possible causes of those variations, presents an analytical model of the morphological features found in earlier qualitative models and numerical simulations, and identifies aspects of the features and patterns that have yet to be resolved.

1. Introduction

We describe the plasma and magnetic field structures in corotating interaction regions (CIRs) and the patterns of turbulence parameters and energetic particles associated with them, focusing primarily on CIR properties in the middle heliosphere,

Space Science Reviews **00:** 173–214, 1999.

between 2 and 8 AU. Complementary to the more comprehensive, tutorial material on these subjects in preceding papers in this issue, the material here extends to topics on the frontiers of research. Sect. 2 addresses the primary morphological plasma and magnetic features of CIRs, ending with a brief summary of how they evolve with distance from the middle to the outer heliosphere. Sect. 3 presents a new analytical model that quantifies these CIR features. Sect. 4 addresses the profiles of turbulence, magnetic field variance, discontinuities, waves, diffusion coefficients, and energetic particles relative to the plasma features and reviews the evolution of some aspects of these profiles with distance from the inner to the middle heliosphere.

2. Morphological Structures

R. F. WIMMER-SCHWEINGRUBER, R. J. FORSYTH, N. U. CROOKER, J. T. GOSLING, P. R. GAZIS, and A. J. LAZARUS

A corotating interaction region, or CIR, is a compression formed as quasi-stationary high-speed solar wind flow runs into slower plasma. Being a consequence of the radial alignment of flows with large speed differences, CIRs are produced almost exclusively within the low-latitude band of solar wind variability, at least in the declining and minimum phases of the solar activity cycle. The leading edge of a CIR is a forward pressure wave that propagates into the slow plasma ahead of it, while the trailing edge is a reverse pressure wave that propagates back into the trailing high-speed flow. CIRs are usually well formed at Earth's orbit. An essential change in their nature, however, occurs at heliocentric distances beyond $\sim$2 AU: the bounding pressure waves steepen into shocks (*e.g.*, Hundhausen and Gosling, 1976, Smith and Wolfe, 1976). CIRs transfer momentum and energy from the fast to the slow wind by accelerating the slow wind and decelerating the fast wind.

The interaction between fast and slow wind within a CIR is centered on the stream interface (*e.g.*, Belcher and Davis, 1971), which separates what was originally fast from what was originally slow wind close to the Sun. The actual compression and deflection of the flow, however, occurs primarily at the forward and reverse pressure waves that bound a CIR. Polarity reversals in the interplanetary magnetic field, which represent crossings of the heliospheric current sheet (HCS), are closely associated with CIRs and stream interfaces, but do not play a fundamental role in the interaction between the high- and low-speed flows. Rather, the HCS serves as a marker of the magnetic control of the solar wind expansion that produces a CIR.

The pattern of flow associated with a CIR corotates with the Sun, even though individual solar wind plasma elements all flow nearly radially out from the Sun. Thus CIRs form spirals in the solar equatorial plane and produce azimuthal as well as radial accelerations (and decelerations) of the flow. In addition, CIRs have

characteristic north-south tilts that are opposed in the opposite solar hemispheres (*e.g.*, Gosling *et al.*, 1993b; Pizzo, 1991). These tilts arise because the solar wind flow pattern close to the Sun typically is inclined with respect to the heliographic equator. As a result, the forward waves in both hemispheres propagate toward and across the equator and produce equatorward accelerations of the slow wind, while the reverse waves propagate poleward to latitudes above the band of solar wind variability and produce poleward accelerations of the fast wind.

Field line geometry in CIRs is an essential aspect of understanding associated energetic particle effects. Fig. 1 illustrates the global magnetic field geometry in the solar equatorial plane assuming that the ambient field there is well approximated by Parker/Archimedean spirals. The field lines enter into the CIR from the upstream sides of the forward and reverse waves and are inclined obliquely to the waves at all heliocentric distances. Since the shocks form at large (> 2 AU) heliocentric distances, well after that portion of the plasma passes through the forward and reverse waves, field lines threading the center of the CIR never intersect the shocks (*e.g.*, Palmer and Gosling, 1978). Departures of the ambient field from pure Parker spirals, for example, those associated with random walk of footpoints in the photosphere (*e.g.*, Kóta and Jokipii, 1983), might modify the geometry illustrated, but suprathermal electron measurements demonstrate that the field geometry is essentially as shown (Gosling *et al.*, 1993a). (See, also, Mason, von Steiger *et al.* (1999) and Scholer, Mann *et al.* (1999) in this issue.)

The following sections explore various aspects of the above morphology, with an emphasis on recent work. For a comprehensive overview of the global morphology outlined above, see the tutorial by Gosling and Pizzo (1999) in this issue.

2.1. Stream Interfaces

Somewhere inside a CIR lies at least one stream interface, separating what was originally kinetically cool, dense, and slow solar wind from the streamer belt (Gosling *et al.*, 1981) from what was originally hot, tenuous, and fast solar wind from coronal holes (Krieger *et al.*, 1973; Gosling *et al.*, 1978). Since it is the interaction of these two types of solar wind that results in a CIR, the stream interface is a defining structure within the CIR. Not all stream interfaces give obvious, discontinuous signatures, however, and only those which give discontinuous signatures form a surface.

Stream interfaces were first observed as flow shears by Siscoe *et al.* (1969) and as discontinuous changes in density, temperature, and wave amplitude by Belcher and Davis (1971). The term "stream interface" was proposed by Burlaga (1974). He attributed interfaces to temperature differences in the corona and their subsequent nonlinear evolution in interplanetary space. Gosling *et al.* (1978) found that the He/H abundance ratio, on average, increases abruptly at the stream interface. They attributed the increase to the different coronal origins of the fast and slow solar wind. Wimmer-Schweingruber *et al.* (1997) confirmed this view. Using

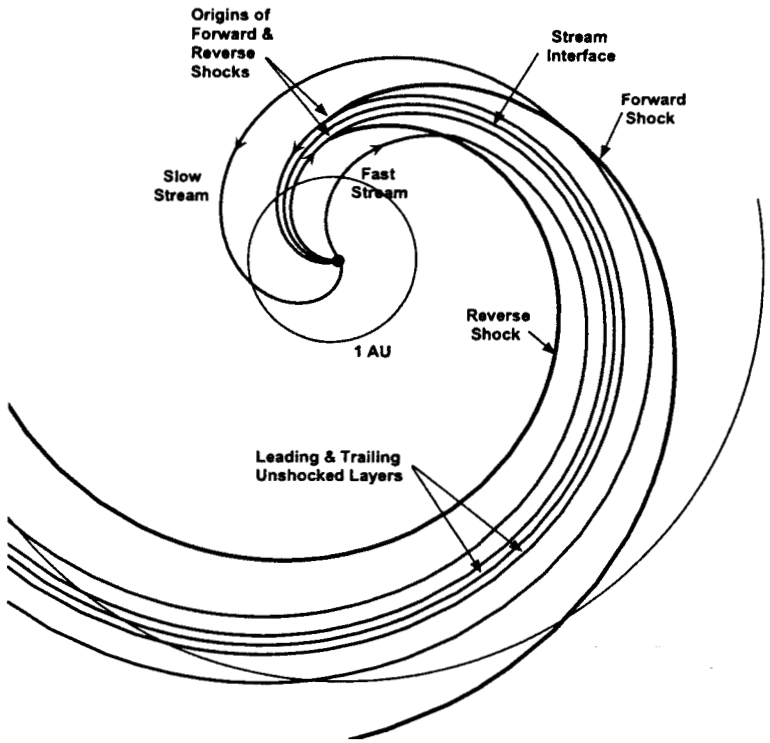

Figure 1. Schematic showing the expected IMF-CIR shock geometry when the ambient field consists of Parker spirals. Flow stream lines and magnetic field lines coincide in a frame of reference corotating with the Sun.

freezing-in temperatures of oxygen and carbon, as well as the low first ionization potential (FIP) to high FIP elemental abundance ratio Mg/O, they showed a distinct compositional change at interfaces.

As a reasonably typical example of a CIR, Fig. 2 shows CIR 7 encountered by Ulysses near 5 AU on its initial southward pass. (See Bame *et al.* (1993), for the numbering scheme of high-speed streams, which is also used for the related CIRs.) From bottom to top, Fig. 2 shows proton number density n_p, speed, kinetic (proton) temperature T_p, specific entropy argument $T_p/\sqrt{n_p}$, normal and tangential flow components (r,t,n coordinates), the α/p ratio, carbon and oxygen freezing-in temperatures, magnetic field latitude θ_B, longitude ϕ_B, and magnitude $|\mathbf{B}|$, and differential speed between α particles and protons. A solid black rectangle in the speed panel indicates an interval of bidirectional electron streaming (BDE) signaling an interplanetary coronal mass ejection (ICME). The CIR is bounded by a forward shock and a reverse pressure wave, marked by vertical dashed lines

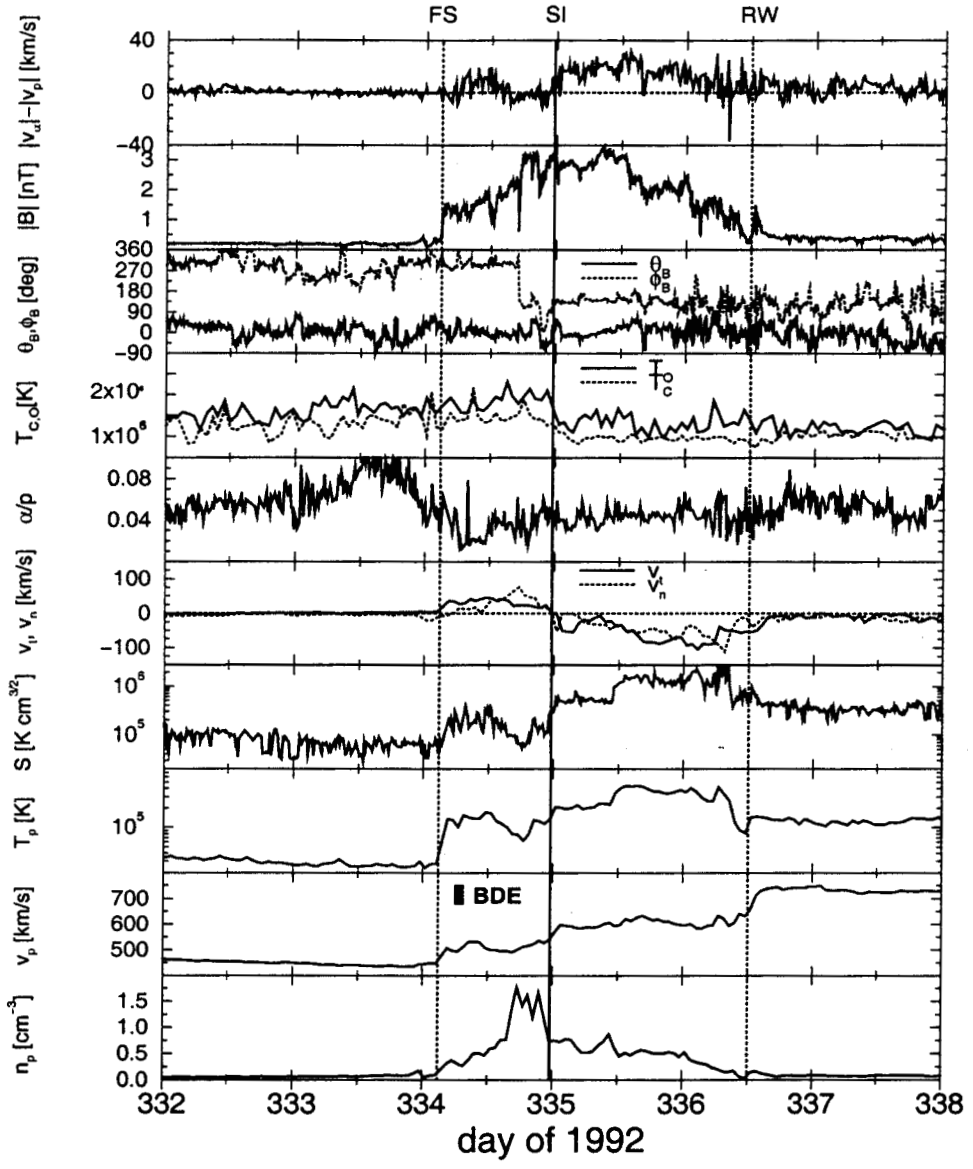

Figure 2. Plasma and magnetic field parameters for CIR 7. See text for discussion.

(FS and RW). Between them, the proton density and magnetic field strength are elevated. At the stream interface (solid vertical line, SI), the density drops, the kinetic temperature rises, and a flow shear is evident, as found in the defining studies mentioned above. (See, also, Gosling and Pizzo (1999).)

The compositional parameters in Fig. 2 ensure that we are seeing material of different coronal origin on either side of the stream interface, as first documented

by Geiss *et al.* (1995). The freezing-in temperatures of C and O exhibit a drop at the stream interface, from typical slow-wind to typical fast-wind values. The same is true for abundance ratios of low-FIP to high-FIP elements, *e.g.*, Mg/O (not shown) (Wimmer-Schweingruber *et al.*, 1997). The α/p ratio is nearly constant in the high-speed wind but very variable in the slow wind (Bame *et al.*, 1977). (Note that the dip in α/p preceding the stream interface is associated with the crossing of the heliospheric current sheet (Borrini *et al.*, 1981), marked by the decrease in ϕ_B.) The compositional aspects of CIRs are discussed in more detail elsewhere in this issue (Balogh, Bothmer *et al.*, 1999). Here we add only that as the CIR evolves, defining signatures like flow shears may fade away with increasing distance, but the immiscibility of the solar wind originating from different regions on the Sun guarantees that the compositional properties will remain largely unaltered.

The top panel in Fig. 2 shows a sudden increase in the speed of α particles relative to the speed of protons at the stream interface, as is often observed there (Gosling *et al.*, 1978; Wimmer-Schweingruber *et al.*, 1997). This differential streaming has been attributed to wave-particle interactions (Neugebauer *et al.*, 1996) or Alfvén wave surfing of the α particles (Asbridge *et al.*, 1976; Marsch *et al.*, 1982) in the fast wind but not in the slow wind.

Summarizing the discussion of Fig. 2, we list the following criteria for identifying stream interfaces: *a*) a drop in density, *b*) a rise in kinetic temperature, *c*) a flow shear, *d*) a change in α/p from typically low (3%) but very variable to typically high (4.7% on average) values, *e*) a drop in freezing-in temperatures, *f*) a drop in low-FIP to high-FIP elemental abundance ratios, and *g*) an onset of differential speed between α particles and protons. Criteria *a*, *b*, and *c* constitute the standard definition of a stream interface, and criteria *d*, *e*, and *f* constitute the more recently emphasized compositional definition. Additional criteria are *h*) a peak in total pressure, discussed by Gosling and Pizzo (1999), and, less reliable, *i*) a magnetic field discontinuity, discussed below. We add here that the same identification criteria apply to stream interfaces on the trailing edges of high-speed streams, going from the originally fast into the originally slow solar wind (Geiss *et al.*, 1995; Burton *et al.*, 1999), although in reverse order, i.e., a rise in density, a drop in kinetic temperature, a rise in freezing-in temperatures, etc.

Stream interfaces have been associated with tangential discontinuities (Gonzalez-Esparza and Smith, 1997; McComas *et al.*, 1998) although the magnetic signature is often ill-defined (Burlaga, 1974; also, see Sect. 4.2.2). In principle, one might only expect a magnetic field discontinuity at a stream interface if the plasma signatures are also discontinuous. Study of the Ulysses data set has revealed that once an interface has been identified using criteria $a - f$, an associated magnetic field discontinuity can be found in most cases. For the 1992–1993 sequence of CIRs, the majority of discontinuities clearly associated with stream interfaces were consistent with being tangential, but there were some exceptions. In particular, at the interface in CIR 7, a clear non-zero normal component was found through the discontinuity, indicated by the changes in ϕ_B and θ_B in Fig. 2.

We close this Section with three brief discussions of cases that deviate from the typical interface pattern either in number of occurrences, lack of some criteria, or association with ICMEs. Firstly, single CIRs can contain multiple stream interface signatures, as found in a study of Ulysses data by Wimmer-Schweingruber *et al.* (1997). Those authors attributed them to multiple crossings of a single, wavy coronal hole boundary. Since CIRs are sandwiched between the slow and fast wind, this interpretation always requires an odd number of stream interfaces in a CIR.

Secondly, although a stream interface was first defined by the concurrent temperature rise and density drop on the leading edge of a high-speed stream (criteria *a* and *b*), and the resulting change in entropy ($\propto T/n^{\gamma-1}$) is a convenient interface marker that incorporates both signatures (Intriligator and Siscoe, 1994), identification by entropy alone can be misleading, even if both criteria *a* and *b* are met separately. For example, sometimes the most pronounced entropy change in a CIR is not accompanied by the expected compositional changes. The entropy rise near 1100 UT on day 335 in Fig. 2 is one such case. Another case, discussed in Sect. 2.2.2, occurred on the trailing edge of an ICME, which may have been its cause.

Thirdly, in what seems like a curious mix of steady-state and transient concepts, some signatures that fit many of the interface criteria occur within ICMEs. Since a CME rising from a helmet streamer moves into the domain of the slow solar wind, and a stream interface is the boundary between the slow and fast wind, one expects an interface to follow an ICME as a CIR corotates past a spacecraft. This pattern has been documented for some cases, for example, by Crooker *et al.* (1999). In contrast, evidence of interfaces within rather than after ICMEs was also found. Interfaces identified by Wimmer-Schweingruber *et al.* (1997) in CIRs 3–6 in the Ulysses series occurred within BDE intervals (see Sect. 2.2.2 for the case for CIR 3). Crooker and Intriligator (1996) found a similar pattern. Although these cases may be nothing more than examples of boundaries in transients with interface-like signatures, they raise the interesting possibility that CMEs are somehow related to interface evolution.

2.2. Sector Boundaries Associated with CIRs

2.2.1. *Relationship to Stream Interface and Shocks*

A sector boundary is a crossing from magnetic field lines of one polarity (originally inward or outward from the Sun) to field lines of the opposite polarity, in other words, a crossing of the heliospheric current sheet (HCS), which is part of the large scale structure of the heliosphere separating the northern and southern magnetic hemispheres. The configuration of the HCS and the streamer belt near the Sun plays a crucial role in the eventual development of CIRs, as described elsewhere in this issue (Forsyth and Marsch, 1999; Gosling and Pizzo, 1999); but, unlike the stream interface boundary discussed above, a sector boundary does not have to be found locally within the compression region of a CIR, although it often is.

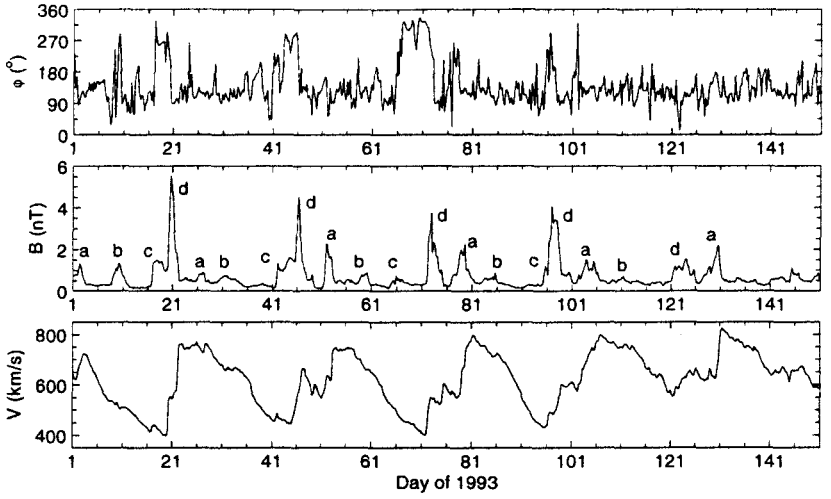

Figure 3. CIRs observed by Ulysses during the first 5 months of 1993. Magnetic field azimuth angle ϕ, field magnitude and solar wind speed are shown. Letters $a-d$ identify recurrent multiple CIRs (from Smith *et al.*, 1993).

Near the Sun the HCS is embedded in the band of slow solar wind associated with the streamer belt. As a natural part of the process of CIR evolution, the forward wave or shock propagates outward into the slow solar wind ahead of the interaction region and eventually overtakes the region of slow wind containing the HCS. Borrini *et al.* (1981) noted that about two-thirds of all well-defined sector boundaries at 1 AU occur within CIRs, and Thomas and Smith (1981) showed that the forward shock had overtaken the sector boundary in the majority of CIRs observed by Pioneer 10 beyond 5 AU. This was also the case for the majority of the CIRs in the sequence observed by Ulysses in 1992–1993, at about 5 AU in the latitude range 13–30°S. Fig. 3, reproduced from Smith *et al.* (1993), gives some examples. Although on this scale the timing is not obvious, the sector boundary crossings into the dominant southern hemisphere polarity, marked by the ~180° decreases in the magnetic field azimuth angle ϕ in the top panel, occurred within the interaction regions marked by the magnetic field compressions labeled *d* in the second panel, after the forward shocks at their leading edges.

Since the sector boundary lies ahead of the high-speed stream driving the CIR, it should always be found preceding the stream interface, in agreement with the observations of Gosling *et al.* (1978). This behaviour is illustrated in Fig. 2, where the sector boundary (ϕ_B, third panel) occurs after the forward shock but before the stream interface. Fig. 4 shows the time duration by which the sector boundary led the stream interface for the 1992–1993 Ulysses CIRs as a function of time, distance and latitude. Apart from CIR 5, which is complicated by the presence of an ICME ahead of it, the sector boundaries and stream interfaces come closer together with

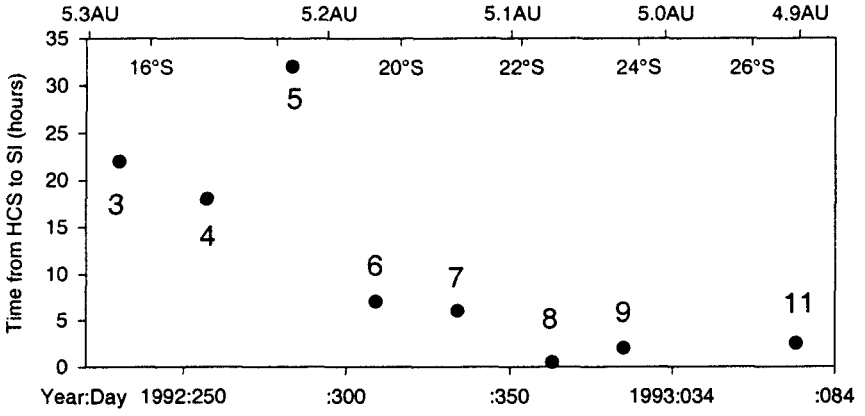

Figure 4. The time duration by which the sector boundary led the stream interface (SI) for CIRs observed by Ulysses during 1992–1993. The heliocentric distance and latitude of Ulysses are shown along the top axis. The CIRs have been numbered using the scheme of Bame *et al.* (1993).

increasing latitude. This behaviour is puzzling for two reasons. Firstly, it is not apparent in the numerical simulations of Pizzo (1994), who modelled the deformation of the HCS by stream interactions. Secondly, it appears to be inconsistent with results from near the ecliptic plane (Siscoe and Intriligator, 1993; Intriligator and Siscoe, 1994) where the HCS and stream interface boundaries were effectively found to coincide within the time resolution of the data (see Sect. 4.5). Further study is needed to resolve these issues.

Note that the magnetic polarity within the high-speed wind behind the stream interface can be used to identify the polarity of the coronal hole from which the stream originated. Thus the high-speed stream driving the CIR in Fig. 2 is of negative polarity and, in fact, was shown to come from an equatorward extension of the southern polar coronal hole (Bame *et al.*, 1993).

2.2.2. *Relation to ICMEs*

ICMEs, the presumed interplanetary ejecta from CMEs, are often found in CIRs, consistent with an intimate association between some ICMEs and the HCS (*e.g.*, Crooker *et al.*, 1998). Expectation of a topological relationship derives from the fact that CMEs are commonly emitted from the helmet streamer belt at the base of the HCS. In many cases, the polarity change that marks HCS passage is effected by a large-scale field rotation in an ICME, making the ICME an integral part of the HCS. Field rotations in ICMEs are usually interpreted as flux rope signatures and called "magnetic clouds" (*e.g.*, Burlaga, 1991).

Both Fig. 2 and Fig. 5 give examples of ICMEs within CIRs. The ICMEs are identified by the BDE intervals, which are primary signatures of magnetically closed structure in the solar wind (*e.g.*, Gosling, 1990). The ICME in Fig. 5 is particularly interesting. Taken as a composite of the three BDE intervals, it contains the field rotation that effects the polarity reversal across the sector boundary. The

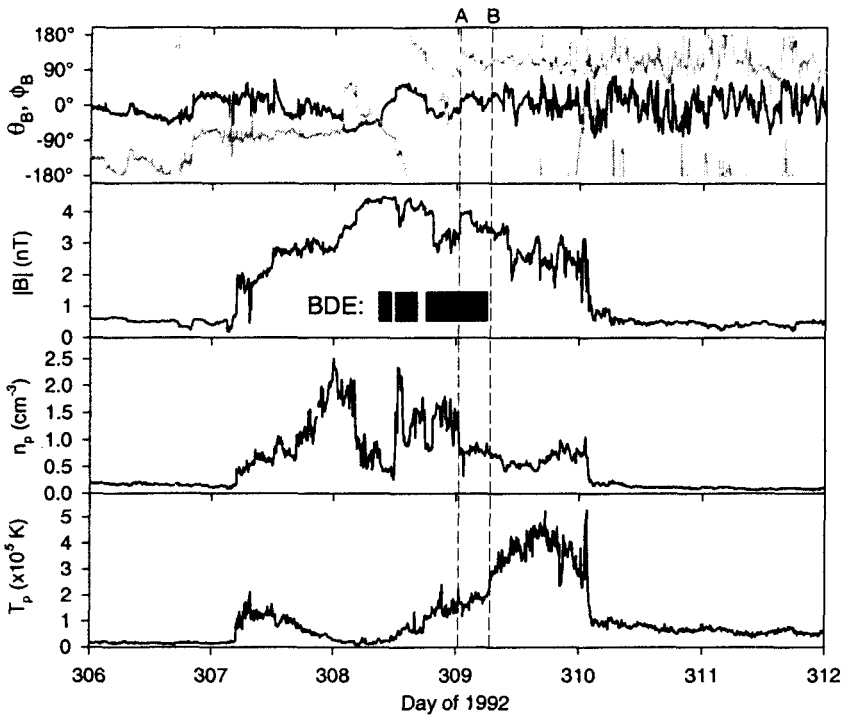

Figure 5. Plasma and magnetic field parameters for CIR 6. The dark bars indicate regions where bidirectional suprathermal electrons (BDE) were observed.

rotation is clearest in the azimuth angle ϕ_B, plotted in gray in the top panel. It begins around 0600 UT on day 308, shortly before the beginning of the ICME, and ends near the end of the day. The ICME, however, continues beyond the rotation to about 0600 UT on day 309. This pattern, identified by Crooker *et al.* (1998) in ISEE 3 data, implies that the ICME is larger than the flux rope.

The ICME in Fig. 5 contains not only the sector boundary but, also, the stream interface, as mentioned in sect. 2.1. The interface was identified by Wimmer-Schweingruber *et al.* (1997) on the basis of compositional criteria and the drop in n_p at line A. It lies at the end of the large-scale field rotation marking the sector boundary, consistent with the expected order between interface and HCS, but in the middle of the BDE interval marking the ICME. Where one might expect the interface, after the ICME at line B, there is an increase in T_p, which creates a pronounced entropy change (not shown) characteristic of an interface; but it is not accompanied by any significant drop in n_p or the compositional criteria for an interface and, consequently, has not been identified as one. The presence of ICMEs in CIRs clearly adds complexity to basic CIR morphology.

2.2.3. *Streamer Belt, Plasma Sheets, and Multiple Current Sheets*

Like ICMEs, high-density structures and multiple current sheet crossings are found in CIRs by virtue of their association with the HCS. The HCS was first revealed as a high-density structure through superposed epoch analysis by Borrini *et al.* (1981) and Gosling *et al.* (1981). These authors identified the structure as the interplanetary signature of the coronal streamer belt. Subsequent studies at higher time resolution have shown that the high-density feature encasing the HCS is often distinct from the general high-density slow wind in which it is embedded. It has higher density, higher β (ratio of gas pressure to magnetic field pressure), and is in pressure balance with the surrounding slow wind (Winterhalter *et al.*, 1994; Bavassano *et al.*, 1997). These studies call the feature the "heliospheric plasma sheet".

Crooker *et al.* (1996b) demonstrated that high-β plasma sheets are general features of complex sector boundaries. In cases where multiple polarity reversals occur, all tend to be encased in plasma sheets. This would be expected if the multiple reversals reflected waves in a single HCS encased by a plasma sheet; but a number of analyses do not support this view (Crooker *et al.*, 1996a,b; Kahler *et al.*, 1998). In some cases the polarity reverses not across the global HCS but across current sheets bounding flux tubes that locally fold back on themselves; yet plasma sheets generally accompany these spatially limited current sheets as well as the HCS. Conversely, there is no distinctive plasma sheet in cases where the current responsible for the polarity change is distributed across a magnetic cloud, as in Fig. 5, since clouds are low-β structures. As for the structure of complex sector boundaries, the data are consistent with an interpretation in terms of multiple current sheets bounding tangled flux tubes.

2.3. MULTIPLE CIRS

Multiple stream interfaces within a single CIR were discussed in Sect. 2.1, and multiple current sheets within a single CIR were discussed in Sect. 2.2.3. To complete our coverage of morphological complexities, we add that CIRs themselves can occur in multiples during passage of a single high-speed stream. Examples can be found in Fig. 3, from Smith *et al.* (1993). The multiple CIRs are labeled $a-d$. Unlike multiple interfaces, they are not confined to the leading edge. They appear to have arisen from a secondary set of streams superposed on the primary stream. Like CIRs in general, multiple CIRs appear to be corotating structures, since, in the case of Fig. 3, they recurred with each solar rotation, as the repetitive labels indicate. Thus, like multiple interfaces, they appear to arise from a wavy coronal hole boundary, with the difference that the boundary need only be approached and not necessarily crossed in the case of multiple CIRs. As a result, not every CIR in a multiple series has a stream interface.

2.4. Evolution with Heliocentric Distance

Corotating interaction regions consisting of forward and reverse shock pairs bounding regions of increased density, temperature, and field strength are dominant structures in the solar wind at heliocentric distances between 2 and 8 AU. At larger heliocentric distances, CIRs undergo significant evolution, and a succession of different types of structure is observed at increasing distances from the Sun.

CIRs spread as they convect outward from the Sun. At heliocentric distances greater than ~5–8 AU, CIRs begin to merge and interact to produce merged interaction regions (MIRs) (Burlaga, 1988; Burlaga *et al.*, 1983; 1985). For most CIRs, this process appears to occur between 5–8 AU, though some CIRs merge closer to the Sun, and a few propagate undisturbed to even larger heliocentric distances. MIRs and their associated shocks appear to be the most common type of interaction structure between ~8 and ~12 AU. Between 10–20 AU, the associated shocks decline in strength to the point where they are difficult to detect and presumably have little effect on the dynamics of the solar wind, and the most common structures in the solar wind become corotating pressure enhancements, which resemble MIRs except for the absence of shocks. At even larger heliocentric distances (>15–20 AU), these corotating pressure enhancements are replaced by broad and irregular enhancements in solar wind density and temperature that are qualitatively different in character from the corotating structures observed closer to the Sun. This succession of structures is described in detail elsewhere in this issue (Gazis *et al.*, 1999).

After 1989, Voyager 2 left the vicinity of the solar equator and began moving to higher latitudes. At heliographic latitudes $\geq 10°$, Voyager 2 observed periodic enhancements in solar wind temperature and speed. These structures were significantly different from the structures observed in the vicinity of the solar equator at comparable heliocentric distances by Pioneer 10. Voyager 2 is headed upstream with respect to the local interstellar medium (LISM) while Pioneer 10 was headed downstream, so it remains to be determined to what extent the differences between Voyager 2 and Pioneer 10 were due to latitudinal gradients, solar cycle variation, or the effect of interstellar pickup ions.

3. An Analytical Model of the Plasma and Field Morphology of CIRs

M. A. LEE

Gosling and Pizzo (1999) and Sect. 2 describe the structure of CIRs based on observations and inferred by both HD and MHD numerical calculations: The pattern of slow and fast wind over the surface of the Sun combined with solar rotation produces radial alignment of slow and fast wind. Where fast wind overtakes slow wind a compression region develops, which, with increasing radial distance

r, develops forward and reverse shocks. The orientation of the stream interface at distance r is determined by the pattern of streams at the Sun and, in turn, determines the deflection of the interacting fast and slow streams in latitude and longitude (Pizzo, 1991). Due to the spherical geometry, the interface normal vector rotates toward the radial direction with increasing r, which together with decreasing Alfvén and sound speeds increases the compression rate at the CIR and reduces the stream deflections. The global structure of the interface determines the global pattern of shock propagation, which becomes more complex with the approach of solar maximum activity.

Thus, the basic physics of CIR formation is well established, both conceptually, based on observations over a large range of latitude and radial distance and during various phases of the solar activity cycle, and quantitatively, based on 1-D (*e.g.*, Hundhausen, 1973), 2-D (*e.g.*, Pizzo, 1991), and 3-D (*e.g.*, Pizzo, 1994) numerical calculations. What is currently lacking, however, is an approximate analytical model which assumes a stream pattern at the Sun and the characteristics of the fast and slow streams and derives interface orientation, stream deflections and shock strengths as functions of latitude and distance r. The model outlined below was developed to fill this need.

The morphology of CIRs is determined by the curve $f(\theta',\phi') = 0$ on the solar wind source surface which divides fast and slow solar wind. The source surface is a sphere of radius r_0 at which the solar wind is approximately radial, free-streaming, and in lateral pressure balance. The angles θ' and ϕ' are the spherical angular coordinates in the frame rotating with the Sun, where θ' is measured from the solar rotation axis. For an ideal CIR, the curve $f(\theta',\phi') = 0$ is independent of time so that the morphology of the CIR is stationary in the corotating frame, as implied by the name. If the fast and slow wind had the same speed V, then the stream interface in the corotating frame would be the surface $f[\theta',\phi' + \Omega V^{-1}(r - r_0)] = 0$, where Ω is the angular speed of the Sun. In the inertial frame the interface surface is given by

$$f[\theta, \phi - \Omega t + \Omega V^{-1}(r - r_0)] = 0 \tag{1}$$

At any point on the surface the normal vector satisfies

$$\mathbf{n} \propto \frac{1}{r}\frac{\partial f}{\partial \theta}\mathbf{e}_\theta + \frac{\partial f}{\partial \phi}\left[\frac{\Omega}{V}\mathbf{e}_r + \frac{1}{r\sin\theta}\mathbf{e}_\phi\right] \tag{2}$$

Equation (1) gives only the approximate location of the interface. If V is the slow solar wind speed and $V + \Delta V$ is the fast solar wind speed, where V and ΔV are assumed to be constant, then the fast solar wind impinges on the interface (Pizzo, 1991). The fast wind is deflected at the interface, which is assumed to be a "free-slip" boundary. The fast wind is also compressed, and a reverse shock is launched back into the fast wind. In response, the slow wind and interface are forced to move, and a forward shock is launched into the slow wind.

If the distance between the shock and the interface is small compared with the spatial scale of the interface, then the CIR (the compressed region between the shocks) is approximately locally planar, with uniform flows in the shocked fast and slow wind. Since the heliospheric magnetic field cannot cross the interface, the field is parallel to the interface and the shock surfaces in this planar geometry. As a result, both shocks are perpendicular shocks, across which the transverse flow is conserved.

Let Regions 1, 2, 3 and 4 be the fast wind, the shocked fast wind, the shocked slow wind, and the slow wind, respectively. In the reference frame of the slow wind, the flow velocities in Regions 1 and 4 are $\Delta V\mathbf{e}_r$ and 0. Since flow transverse to $\mathbf{n}$ is conserved at the shocks, the transverse flows in Regions 2 and 3 are $\Delta V[\mathbf{e}_r - (\mathbf{e}_r \cdot \mathbf{n})\mathbf{n}]$ and 0, with large shear at the interface. Let the normal component of the flow in Regions 2 and 3 be v_2 (they must be the same since the interface is a tangential discontinuity). In the inertial frame, the flows in the four regions are then

$$1: \quad (V + \Delta V)\mathbf{e}_r \tag{3}$$

$$2: \quad V\mathbf{e}_r + v_2\mathbf{n} + \Delta V[\mathbf{e}_r - (\mathbf{e}_r \cdot \mathbf{n})\mathbf{n}] \tag{4}$$

$$3: \quad V\mathbf{e}_r + v_2\mathbf{n} \tag{5}$$

$$4: \quad V\mathbf{e}_r \tag{6}$$

In Regions 2 and 3, there exist flows transverse to the radial direction

$$2: \quad \mathbf{v}_{T2} = -(v_1 - v_2)[(\mathbf{e}_\phi \cdot \mathbf{n})\mathbf{e}_\phi + (\mathbf{e}_\theta \cdot \mathbf{n})\mathbf{e}_\theta] \tag{7}$$

$$3: \quad \mathbf{v}_{T3} = v_2[(\mathbf{e}_\phi \cdot \mathbf{n})\mathbf{e}_\phi + (\mathbf{e}_\theta \cdot \mathbf{n})\mathbf{e}_\theta] \tag{8}$$

where $v_1 = \Delta V(\mathbf{e}_r \cdot \mathbf{n})$. These expressions give the azimuthal and meridional flows characteristic of CIRs. A sequence of observers in the radial direction would measure an interface speed equal to $V + v_2(\mathbf{e}_r \cdot \mathbf{n})^{-1}$.

Since the reverse shock is compressive, $v_1 > v_2$. It is then an immediate consequence of equations (7) and (8) that transverse flows in Regions 2 and 3 are antiparallel. The ratio of the flow magnitudes is $|\mathbf{v}_{T2}||\mathbf{v}_{T3}|^{-1} = (v_1 - v_2)/v_2$. In either Region 2 or Region 3, the ratio of the azimuthal flow speed to the meridional flow speed is $(\mathbf{e}_\phi \cdot \mathbf{n})/(\mathbf{e}_\theta \cdot \mathbf{n})$, which is determined by the structure of the stream interface at the source surface through equation (2).

At this stage, v_2 is unknown. The speed, density, pressure and magnetic field strength in the fast and slow wind are, in principle, known. In addition to v_2, there are 8 unknowns: the density, pressure and field strength in Regions 2 and 3; the speeds of the forward and reverse shocks relative to the slow solar wind. There are 9 conditions relating these quantities: continuity of mass, momentum and energy flux and electric field at each shock; continuity of total pressure at the interface. The 9 conditions determine the 9 unknowns. It can be shown that the 9 conditions combine to yield one implicit equation for a single unknown, which, in general, must be solved numerically.

The case of weak compression, appropriate to the early formation of the CIR at small r, may be addressed analytically. If $v_1 << V_{f1}$, where V_{f1} is the MHD "fast" speed in the fast wind, then the compression ratios at the forward shock (X_F) and the reverse shock (X_R) are close to unity, and the implicit equation may be linearized in v_1/V_{f1} and solved. The solution yields for the following key parameters

$$X_R = 1+\rho_4 V_{f4} v_1 V_{f1}^{-1}(\rho_1 V_{f1}+\rho_4 V_{f4})^{-1} \quad (9)$$

$$X_F = 1+\rho_1 V_{f1} v_1 V_{f4}^{-1}(\rho_1 V_{f1}+\rho_4 V_{f4})^{-1} \quad (10)$$

$$v_2 = \rho_1 V_{f1} v_1 (\rho_1 V_{f1}+\rho_4 V_{f4})^{-1} \quad (11)$$

where ρ_1 and V_{f1} are the mass density and"fast" speed in the fast wind and ρ_4 and V_{f4} the corresponding quantities in the slow wind. The radial speed of the interface is

$$V + v_2(\mathbf{e}_r \cdot \mathbf{n})^{-1} = V + \rho_1 V_{f1} \Delta V (\rho_1 V_{f1}+\rho_4 V_{f4})^{-1}. \quad (12)$$

Although the expressions in equations (9) - (11) are derived under the assumption of weak compression, it can be shown that they are approximately valid for the stronger compression [$v_1/V_{f1} = O(1)$] relevant for CIRs.

Many of these results may be interpreted simply as a consequence of momentum conservation. Equation (11) expresses the requirement that, viewed from Region 2, the **n**-component of momentum is lost from the fast and slow wind at the same rate, so that the interface remains at rest. The compression ratios then follow immediately from mass conservation at each shock wave. Similarly the ratio of the transverse (to the radial) flow magnitudes in Regions 2 and 3, using equation (11), gives

$$\rho_1 V_{f1} |\mathbf{v}_{T2}| = \rho_4 V_{f4} |\mathbf{v}_{T3}| \quad (13)$$

The width of Region 2 is proportional to V_{f1}, and to first order in v_1/V_{f1} the transverse momentum density in that region is $\rho_1|\mathbf{v}_{T2}|$. Thus equation (13) expresses the transverse momentum balance of the oppositely directed transverse flows in Regions 2 and 3.

The results presented are based on (1) the heliospheric structure of the stream interface arising from the pattern of fast and slow solar wind streams near the Sun, and (2) the quasi-planar impinging of the fast wind on the slow wind over the compressional portions of the stream interface. The rarefaction regions do not produce CIRs. This simple basis provides several interesting analytical results concerning the structure of CIRs: the orientation, given by **n**; the deflection of the fast and slow solar wind streams; the compression ratios of the forward and reverse shocks; the speeds of the two shocks (not given explicitly in this brief description), which determine the relative thicknesses of Regions 2 and 3; the radial speed of the stream interface. The results describe the development of the CIR as **n** turns from an $\mathbf{e}_\theta$ or $\mathbf{e}_\phi$ orientation (depending on the tilt of the interface at the solar wind source surface) into the radial direction with increasing r (see equation (2)). The

analysis is no longer valid when the CIR becomes too thick or the forward and reverse shocks interact. The thick CIR is no longer planar, the flow varies within Regions 2 and 3, and the shocks are no longer perpendicular shocks. The fact that the forward and reverse shocks observed by Ulysses are not nearly perpendicular is an indication that the planar ansatz is approximate. Nevertheless, this simple model provides a useful conceptual framework for the plasma and magnetic structure of CIRs within about 5 AU of the Sun. The expressions derived above provide approximate analytical expressions, based essentially on momentum balance and an idealized planar geometry, for CIR orientation, stream deflections, interface motion, and forward and reverse shock strengths. The expressions reveal how these quantities depend on stream speed, density, and sound and Alfvén speeds, and the orientation of the stream interface at the Sun. The analytical expressions should allow observers to interpret their observations semi-quantitatively, without having to rely on numerical calculations necessarily restricted to specific parameters and idealized geometries. A more thorough exposition of the calculation, including two specific choices for the form of the stream interface near the Sun, is presented in Lee (1999).

4. Turbulence, Discontinuities and Waves, and Their Relation to Energetic Particles

T. S. HORBURY, B. T. TSURUTANI, E. C. ROELOF, V. BOTHMER,
D. S. INTRILIGATOR, G. L. SISCOE, J. R. JOKIPII, and I. G. RICHARDSON

4.1. INTRODUCTION

The complex interactions between magnetic field fluctuations and energetic particles within and around CIRs are not well understood. While the subject appears to be a simple one, since the trajectory of a charged particle in an electromagnetic field is well known, several factors make this problem more complex in the heliosphere. Firstly, the magnetic field is by no means constant: there are variations on essentially all scales as a result of waves, turbulence, shocks, discontinuities and so on. Secondly, the energy densities of the particles and fields are often comparable, so that variations in the particles cause variations in the field which, in turn, alter the particle behaviour.

Despite these difficulties, considerable progress has been made in describing these interactions in a statistical sense. In this section, variations in magnetic field fluctuations and energetic particles within and around CIRs are described together. In Sect. 4.2, a single CIR is considered in some detail, and the relationships between turbulence, discontinuities, energetic particles and large scale structure are discussed. In Sect. 4.3, the theory of wave-particle interactions is introduced and applied to measurements within the example CIR. Of central importance in these

sections is particle diffusion perpendicular to the magnetic field, and further aspects of this process are discussed in Sect. 4.4. The relationship between the large scale structure of CIRs and energetic particles within them is discussed in Sect. 4.5, Sect. 4.7 describes possible causes of the reduced energetic particle flux near stream interfaces, and, finally, Sect. 4.7 discusses the changes in particle and fluctuation signatures with distance as CIRs develop and travel away from the Sun.

4.2. A "TYPICAL" CIR

In describing the interactions between fluctuations and particles within CIRs, it is helpful to consider a typical event. While distance, latitude and time variations in the solar wind mean that there is no such thing as a typical CIR, we have attempted to identify one event which has clear, simple variations. We have chosen a CIR encountered by Ulysses in 1993, at 5.0 AU and 24°S, which is representative of those observed at heliocentric distances of several AU, with both forward and reverse shocks: this is CIR 9 in the numbering system based on the classification of high speed streams encountered by Ulysses (Bame *et al.*, 1993). CIRs 6 and 7 of this sequence, encountered at similar latitudes and distances, are discussed earlier in this chapter. CIR 9 was chosen here because of the relatively simple fluctuation and energetic particle variations through the event, although it has a rather more complex structure in composition measurements than CIRs 6 and 7.

Horbury and Schmidt (1999) described the general morphology of waves and turbulence associated with CIRs earlier in this issue, and we refer the reader to that paper for an introduction to the subject. Here we first present a chronological description of bulk plasma and magnetic field parameters, fluctuation power and discontinuities through the CIR, then describe the energetic particle variations. Finally we discuss the correlations in fluctuations and energetic particle variations and their causes.

4.2.1. *Turbulence and waves*

Fig. 6 presents a range of physical parameters between 1993 days 19 and 23. The bottom five panels show bulk parameters: proton temperature T; proton number density N_p; solar wind speed V_r; magnetic field azimuthal angle ϕ; and field magnitude $|\mathbf{B}|$. The top four panels are diagnostics of fluctuations. Total component power (panel 1) is the sum of magnetic field power in all three components in a wavenumber range from 6.5×10^{-5} to 1.3×10^{-4}km^{-1}: fluctuations on these scales are typically turbulent at these solar distances. Each point corresponds to one 15-min interval of data over which the values are calculated. Field-aligned anisotropy (panel 2) is the ratio of power perpendicular to the mean field direction to that parallel, on the same range of scales, and is plotted logarithmically. In general, power is greater perpendicular to the field in MHD turbulence, although large amplitude shock-generated turbulence is often more isotropic. The ratio of power in field components to that in the field magnitude (panel 3, also on a logarithmic

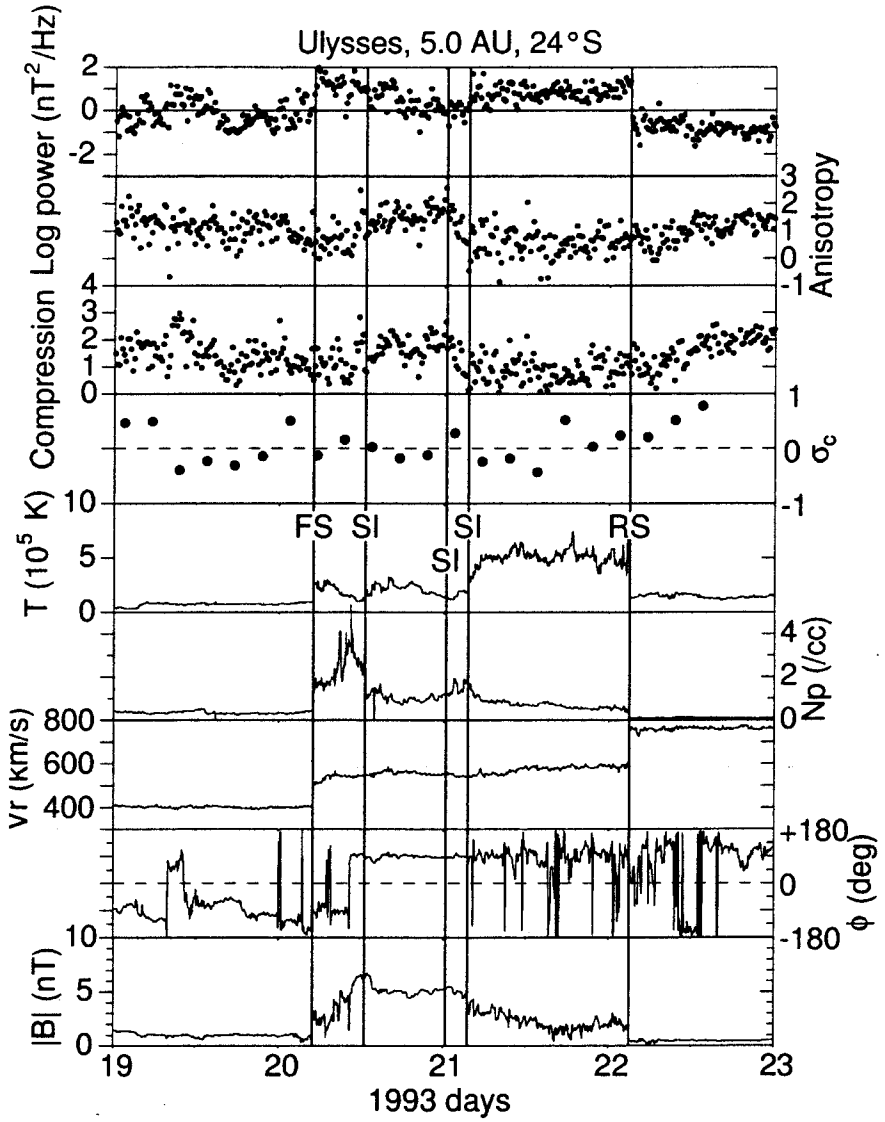

Figure 6. Magnetic field, bulk plasma and fluctuation variations in a CIR 9 encountered by Ulysses at 5.0 AU and 24°S. Times of the forward and reverse shocks (FS and RS) and 3 identified plasma composition changes are marked by vertical lines.

scale), again for the same scales, is a proxy for the level of compressive fluctuations. Low values indicate relatively large variations in field magnitude and, hence, probably density, compared to field fluctuations as a whole. Thus, low values represent high compressibility. Normalised cross helicity (σ_c, panel 4) is a measure of the dominance of Alfvén waves in the fluctuations and is calculated here on hourly scales. Values near +1 indicate a dominant population of Alfvénic

fluctuations propagating away from the Sun in the solar wind frame; values near -1 correspond to inward-propagating waves. Also marked on Fig. 6 are the times of the forward and reverse shocks bounding the CIR and the three stream interfaces (slow/fast, fast/slow and slow/fast) identified using the SWICS composition instrument (Wimmer-Schweingruber *et al.*, 1997).

Fluctuations in undisturbed high-speed wind (far right of Fig. 6) tend to be anisotropic, with small variations in field magnitude and high σ_c. These are dominated by Alfvén waves propagating antisunward, undisturbed since leaving the solar corona. Conditions in fast wind tend to be rather steady compared to those in slow wind. Indeed, fluctuations in the slow solar wind upstream of the forward shock are clearly rather variable, on a scale of several hours. Both power levels and compressibility levels vary by at least two orders of magnitude, although anisotropies are more steady, allowing for measurement variability, with around an order of magnitude more power perpendicular to the field than parallel. There are large changes in σ_c, including a period of dominant inward propagation. Such variability is typical of slow wind. After the beginning of day 20, corresponding to approximately 7×10^6 km upstream of the forward shock, the fluctuations change significantly and progressively towards the shock: power levels rise by around an order of magnitude, and they become more isotropic and more compressive. This power increase is a result of waves generated by streaming particles accelerated by the shock. Downstream of the shock, power levels rise dramatically as a result of shock-generated fluctuations. Values of σ_c are near zero, indicating the presence of a mixture of wave modes. The sector boundary was encountered soon afterwards, around hour 10 of day 20. A stream interface (SI) at 1230 UT of day 20 is associated with a decrease in proton number density and clearly corresponds to a change in the fluctuations, with lower powers, larger anisotropies and lower compressibility following the SI.

Around hour 16 of day 20, there is another change in the fluctuations, with a drop in power levels and increased anisotropy. This may mark the point at which the forward shock "switched on," that is, the forward compression wave within the CIR steepened to form a shock. Plasma upstream of this point (encountered earlier by the spacecraft) would therefore be shocked, with higher turbulence levels, and that downstream would have encountered only a wave not a shock, so have lower turbulence levels. However, this change in fluctuations may also simply represent a different original fluctuation population, reflecting variability like that seen in slow wind upstream of the shock. (See Gosling and Pizzo (1999) for more discussion of this point.)

The small region bounded by two stream interfaces at 0030 UT and 0400 UT on day 21, although identified as being slow wind using composition measurements, appears from its fluctuation signatures to be a transition between the regions on either side. Power levels are similar to those upstream, while anisotropy and compression values vary across the region. The σ_c is high, indicating a dominant population of outward-propagating Alfvén waves.

Around 0400 UT, Ulysses passed into what was originally high-speed wind, experiencing fairly uniform conditions until the reverse shock early on day 22. Power levels in this region of the CIR were high, with a high level of compression. Plasma and field parameters were also noticeably more disturbed. After the reverse shock, there was a gradual transition, over a period of around 12 hours, to normal high-speed wind fluctuations. As with the forward shock, this transition is the result of locally generated waves, with a low cross helicity and high compression levels.

We stress that variations in fluctuations through the CIR are caused by a combination of initial conditions, that is, the population of fluctuations in the different regions in the corona, and local environment, for example, shocks and compressions. Typically, variations in the bulk plasma or composition are accompanied by changes in the fluctuations, resulting in a very complex environment in which energetic particles propagate. In addition, non-thermal particles measured near and within a CIR have often been accelerated in regions far removed from the measurement site and then guided there by the magnetic field. As a result, the relationship between energetic particles and magnetic field fluctuations is complex.

4.2.2. *Discontinuities*

One of the fundamental microstructures present in the solar wind is directional discontinuities, sharp angular changes in the interplanetary magnetic field directionality (Colburn and Sonett, 1966). Relative to CIRs, some of these microstructures form the basic morphological features, and some may affect particle transport. Theoretically there can be several types: rotational (RDs), tangential (TDs) and shocks (fast, intermediate and slow). Shocks and shock effects on particles are discussed elsewhere in this issue. RDs are sharply kinked fields or short wavelength Alfvén waves. As such, they may be involved in scattering charged particles as the particles propagate from one region to another. TDs separate plasmas and fields of different types. Particle transport across large scale TDs is not expected to occur. TDs are simply convected by the solar wind.

This section highlights the discontinuous field changes in CIRs and, at the same time, illustrates the problems in determining discontinuity properties in spacecraft data. Directional discontinuities are identified from magnetic field data using a computerized method applied to 1-min average vectors, as described in Tsurutani and Smith (1979). Once discontinuities are identified, high-time resolution analyses are used to determine the normal direction, the magnetic field component along the normal (B_N), and the larger field magnitude on either side of the discontinuity (B_L). Using these parameters, we apply the Smith (1973a; b) method to identify whether the discontinuities are tangential, rotational or have properties of both.

Fig. 7 shows the number of discontinuities identified in successive 6-hr periods within and around CIR 9. Rates are particularly high in the high-speed wind behind the CIR and in the shocked plasma within the CIR. This is due to the presence of nonlinear Alfvén waves in the high-speed wind, whose origin is a coronal hole (Tsurutani *et al.*, 1995).

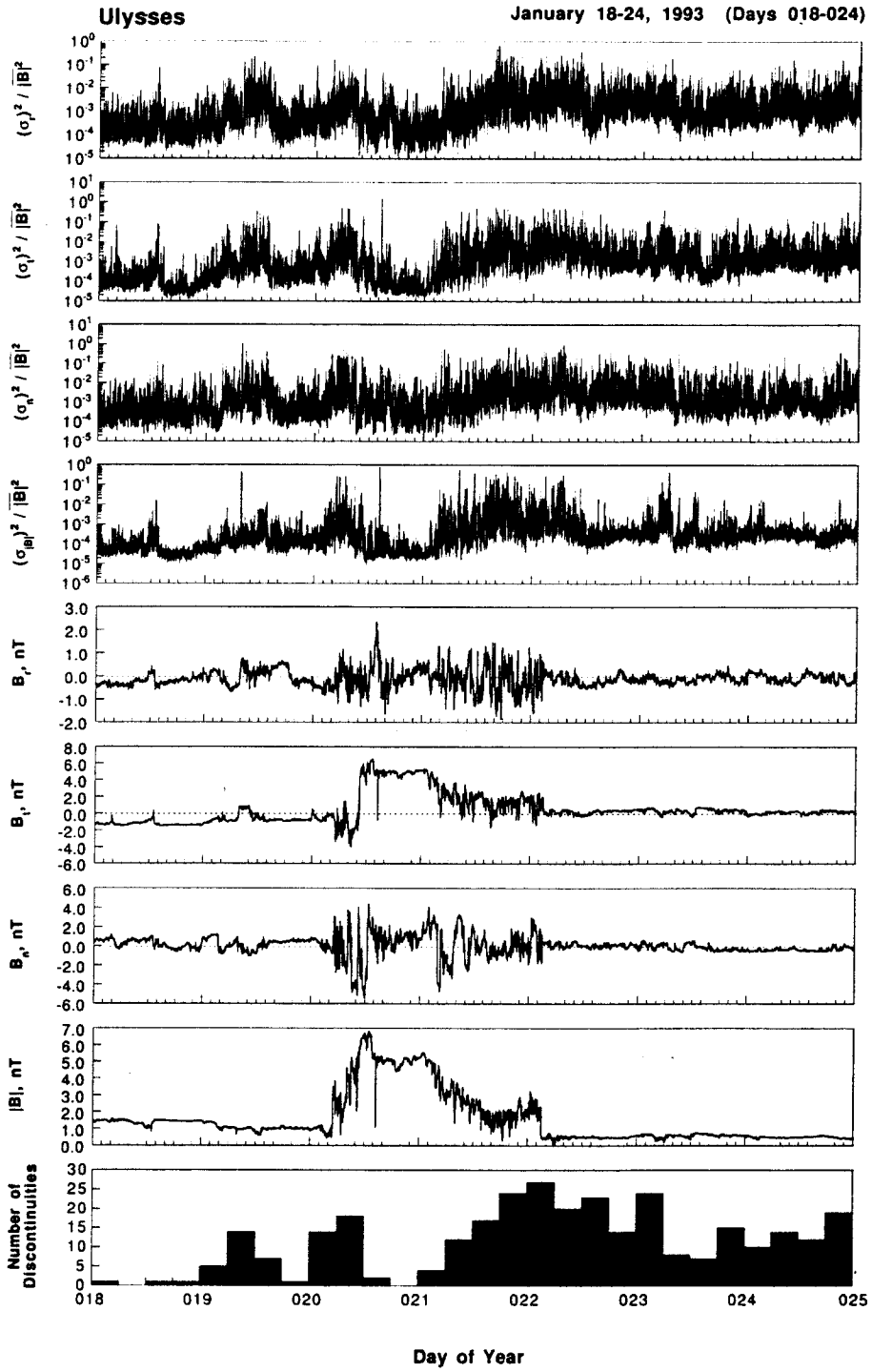

Figure 7. Normalised variances and discontinuity occurrence rates around CIR 9. The normalised variances shown are calculated on a spacecraft scale of 1 minute.

Perhaps the most interesting discontinuities are the ones at the stream interface shown in Fig. 8 (see, also, Sect. 2.1 for a discussion of the relationship between interfaces and discontinuities). Wimmer-Schweingruber *et al.* (1997) identified an ion compositional change at ~1230 UT. From ~1220 to ~1250 UT, there is a large-scale field directional rotation in the B_1 component. However in the field magnitude, there are six prominent field decreases and increases (discontinuities). These are labeled in Fig. 8. Each of the six events has been analyzed using the minimum variance technique. Are these TDs and do they block particle transport across field lines?

Many of the discontinuities have complex properties. Event 1 has a normal orientation 13° relative to the magnetic field, identifying it as a rotational discontinuity. It is a little unusual, however, in that there is a distinct magnetic field magnitude change across the structure ($\Delta|B|/B_L = 0.06$). The second event at 1223 UT is a discontinuity that has both RD and TD properties. There is little or no field rotation across this discontinuity. It would not have been selected as a directional discontinuity by the Tsurutani-Smith method. Event 3 is a rotational discontinuity with a significant magnitude change. For event 4, the interval 1230 to 1238 UT was analyzed. This discontinuity is located in the center of the large scale rotation. This discontinuity has the properties of both a RD and a TD: $B_N/B_L = 0.02$ and

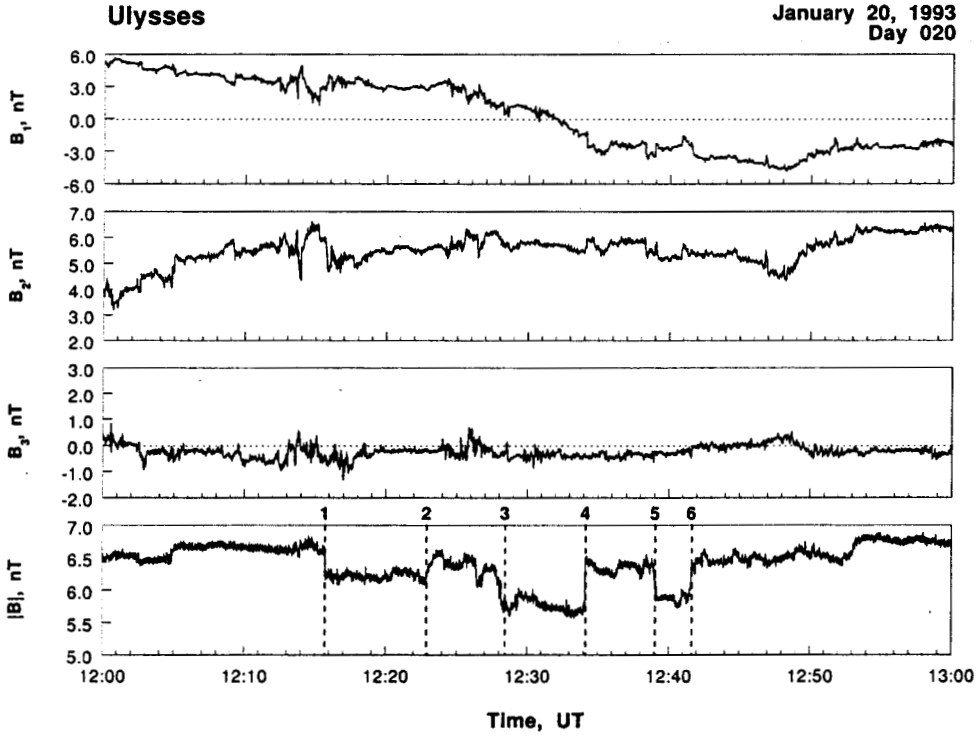

Figure 8. Discontinuities near a stream interface in CIR 9.

$\Delta|B|/B_L = 0.1$. For this event, the angle between the discontinuity normal and the ambient magnetic field is $\theta_{kb} = 89°$. Finally, events 5 and 6, like event 2, have both RD and TD properties.

Reconnection could be occurring across the broad field rotation area containing event 4. Evidence of plasma jetting and heating could tell us if this is occurring or not. The presence of such microstructure within the large field rotation indicates that for this case, there is not a simple TD bounding the two different plasmas. The large scale field tells one that as well.

It is, of course, impossible to unambiguously identify a discontinuity in spacecraft data, and, as a result, various criteria, subjective or objective, are used to select field changes which appear to be discontinuous. The above analysis of the discontinuous field events near the stream interface illustrate the difficulty. While some events appear to satisfy the criteria for MHD discontinuities, others do not. Without more data, the nature of these events remains unclear.

4.2.3. *Energetic particle features*

Fig. 9 shows energetic particle variations across CIR 9 and compares them with parameters repeated from Fig. 6. In the upper panel are one-hour averages of the intensities of the following species of energetic particles measured by the Ulysses/HI-SCALE detectors: 53-103 keV electrons (de2); 480-966 keV protons (w1); 56-78 keV ions (p1); 214-337 keV ions (p4). All ions of approximately the energies specified are counted in the "p" channels from the solid-state detectors, but protons dominate the rates in these channels in the vicinity of CIRs. The three proton channels have very similar histories, and their intensities (cm^{-2} s sr MeV) are well-ordered inversely by energy: p1 with the highest energy, then p4, and finally w1. The electron channel (de2) has a high background and, thus, overlays the proton channels. No background corrections were applied to the intensities of any of the channels in this plot.

There is clearly a general correlation within the CIR between the proton intensities and the level of power in the magnetic fluctuations and a general anticorrelation between the proton intensities and fluctuation anisotropy or compressibility (see discussion of Fig. 6). The intensities of these low-energy protons rise shortly before the arrival of the forward shock and drop soon after the passage of the reverse shock. On the other hand, there is no increase in electron intensity associated with the leading portion of the CIR (between the forward shock and the stream interfaces), and the gradual rise of electron intensity from the stream interfaces to the reverse shock is sustained at a remarkably constant level well after the passage of the reverse shock. Electrons observed well before or after the shocks bounding the CIR are reaching the spacecraft along field lines remotely connected to a distant portion of the CIR (Simnett and Roelof, 1995) and thus probe the properties of the CIR at that distant location.

Within the CIRs, the contrast between the intensity histories of the low-energy protons and the fast electrons is a graphic demonstration that the behaviour of

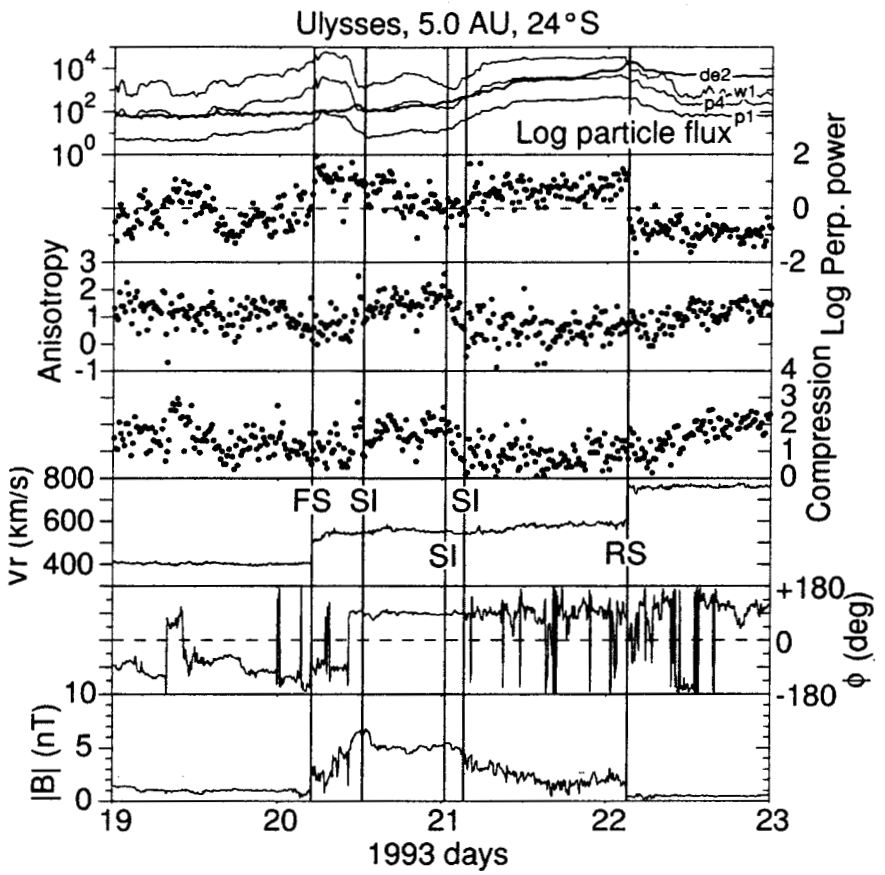

Figure 9. Top panel: Intensities (/cm^2 s sr MeV) of energetic particles from the HI-SCALE detectors on Ulysses: electrons 53-103 keV (de2); protons 480- 966 keV (w1); ions 56-78 keV (p1); ions 214-337 keV (p4). *Lower panels*: Magnetic field fluctuation parameters, solar wind speed, and magnetic field azimuth angle and magnitude, repeated from Fig. 6.

energetic particles associated with CIRS cannot be characterized by any subset of energies or species. Elsewhere in this issue, Kunow, Lee *et al.* (1999) demonstrate that the time histories of the intensities are highly energy-dependent, even within a given species, and that the ordering is more with particle velocity than with energy. Kunow, Lee *et al.* (1999) also argue that it is the lowest energy protons (<1 MeV) whose behaviour is most closely related to plasma and magnetic field parameters in that there is a correlation between 60 keV proton intensities and plasma temperature. This correlation is not observed in the intensities of higher energy protons (>1 MeV), whose different behaviour is reported in Sect. 4.5.

The resolution of the different ordering of intensities of protons above and below 1 MeV may be found in treating the lower energy protons as a suprathermal tail of the thermal plasma and, thus, strongly affected by the plasma parameters. Nonetheless, this suprathermal tail can still propagate away from its acceleration

source along field lines. The higher velocity particles ($\beta > 0.1$), *e.g.*, 50 keV electrons and 10 MeV protons, are much faster than 60 keV protons ($\beta = 0.01$) and obviously have undergone further acceleration to energies well above the suprathermal tail of the plasma. Therefore the modes of both acceleration and propagation may be quite different for the suprathermal and the fast particles (see Sect. 4.5). Further research should reveal the nature of the transition in characteristics from slow to fast particle distributions as well as their different ordering with respect to the plasma and magnetic field structures within CIRs.

4.3. WAVE-PARTICLE INTERACTIONS

To address how particles distribute themselves in CIRs, their means of transport must be understood. In the next two sections we discuss transport processes at the particle gyroradius scale and at the scale of magnetic fluctuations, respectively.

Theoretical expressions have been developed for both parallel pitch angle diffusion (due to resonant scattering) and cross-field diffusion (again assuming resonant pitch angle scattering). The expressions assume parallel propagating transverse waves. To date, the role of nonlinear waves, phase-steepened waves and mirror mode structures have not been theoretically modelled. Since all three types of waves and structures are present in CIRs, we encourage such efforts in the future.

Since our main concern here is the scattering of energetic ions and electrons, we will focus on the particle resonant interactions with the magnetic component of electromagnetic waves. This factor is generally much larger than the interaction with electric components. From Kennel and Petschek (1966), the pitch angle diffusion rate is:

$$D^{\pm}_{\alpha\alpha} = \left(\frac{B_w}{B_0}\right)^2 \Omega^{\pm}_g \tag{14}$$

where B_w is the wave amplitude, B_0 the field magnitude and $\Omega^{\pm}_g$ the particle gyrofrequency. The quantity $(B_w/B_0)^2$ can be calculated from magnetic field variances and is known as "normalized variance." Normalised variances are shown in Fig. 7 calculated on a spacecraft time scale of 1 min. In general, since they are a measure of wave power, they vary in a similar way to the power levels shown in Fig. 6. Normalization by the square of the field magnitude, however, produces some difference: for example, the precise shock times are much less clear in the normalized variances than in the power levels of Fig. 6.

To determine the resonant wave power, one must determine the frequency from the cyclotron resonant condition:

$$\omega - \mathbf{k} \cdot \mathbf{V} = \Omega^{\pm}_g \tag{15}$$

where ω is the wave frequency, $\mathbf{k}$ is the wave vector, and $\mathbf{V}$ is the particle instantaneous velocity vector. One can make a first-order simplification by assuming the waves are propagating parallel to $\mathbf{B}$. This yields:

$$V_{ph} \pm V_{\parallel}^{\pm} = \frac{\Omega_g^+}{\omega} V_{ph} \tag{16}$$

where V_{ph} is the Alfvén speed. V_{ph} is $\approx$50 - 70 km/s in the solar wind at Ulysses distances from the sun, and $V_{\parallel}^{\pm}$ are the parallel velocity vector components of the ions (+) and electrons (-).

The cross-field diffusion rate $D_{\perp}^{\pm}$ due to resonant-wave particle interactions has been derived by inlineciteTsurutaniandThorne1982. Assuming a diffusion rate much less than the Bohm rate for the magnetic component of the waves, one has:

$$D_{\perp}^{\pm} \approx 2 \left(\frac{B_w}{B_L} \right)^2 D_{max} \tag{17}$$

where $D_{max} = E_{\perp} c / 2eB_0$, the Bohm rate, $E_{\perp}$ is the perpendicular particle kinetic energy, c the speed of light, and e the electronic charge. At the maximum, or Bohm rate, the particles diffuse a gyroradius in distance every cyclotron period.

To illustrate the results, the pitch angle scattering rate and cross-field diffusion rate for resonant protons will be calculated. From Fig. 6, the average field magnitude is $\sim$2 nT. Thus $\Omega_g^+ \approx 2 \times 10^{-1}$ rad s^{-1}. We calculate the resonant particle (parallel) energy in the spacecraft frame of reference. The Alfvén speed is $\sim$50 km s^{-1}, which is negligible compared to the solar wind speed of $\sim$500 km s^{-1}. Thus from the resonance condition, we find that $\sim$6 MeV protons strongly interact with these waves.

From Fig. 7, $\sigma_w^2 / B_0^2 \approx 10^{-2}$ for 1-min variations in B_T, in the trailing portion of the CIR, where the normalized variances are particularly high. We note that at times these values can be an order of magnitude higher. Using the lower estimate, from equation (14) we find a scattering time, the reciprocal of the diffusion rate, $T_{sc} \approx 500$ s. The gyroperiod is $\sim$30 s. Thus the protons are scattered once every $\sim$20 gyroperiods. This corresponds to weak pitch angle diffusion. The particles are simply scattered by the waves, and very little diffusion in particle energy takes place.

The cross-field diffusion rate is $\approx 2 \times 10^{-2} D_{max}$ or 2.0% of the Bohm diffusion rate. These particles thus have limited access to neighboring magnetic fields.

We previously noted that the normalized variances were higher by an order of magnitude in places. Thus for these spatial regions, low level particle energization and more rapid cross-field diffusion should be taking place.

At the end of day 20 and beginning of day 21, the normalized variances are at a minimum. The normalized values range from 10^{-5} to 10^{-4} nT^2/Hz, power levels three orders of magnitude below that discussed previously. The pitch angle scattering rates and cross-field diffusion rates are proportionally lower in this part of the CIRs. Thus one would expect the 6 MeV protons to have long mean free

paths and very little access to neighboring magnetic field lines (essentially no cross-field diffusion) in this region of the CIR.

4.4. General Picture of the Diffusion of Energetic Particles Perpendicular to B

Since the magnetic field is turbulent and fluctuates over a broad range of length scales, it is common to define the perpendicular diffusion coefficient $\kappa_\perp$ as the coefficient for diffusion normal to the average rather than local magnetic field. This distinction is important, as will be seen below.

The picture of perpendicular transport which has developed over the years may be summarized as follows. If $\lambda_\parallel = 3\kappa_\parallel/w$ is the parallel mean free path determined by scattering, where w is particle speed, then the classical kinetic theory expression for the ratio of perpendicular to parallel diffusion is

$$\frac{\kappa_\perp}{\kappa_\parallel} = \frac{1}{1+(\lambda_\parallel/r_c)^2}, \tag{18}$$

where r_c is the particle gyroradius in the average magnetic field. For typical values of $\lambda_\parallel$ this is very small for low energy ions, and for this reason it is often neglected entirely.

Some thirty years ago it was pointed out that the random walk, or braiding, of the magnetic lines of force due to the turbulence in the magnetic field could provide a large contribution to the perpendicular diffusion (for a review, see, *e.g.*, Jokipii, 1971). In this view, the particles tend to follow the lines of force as they meander in the direction normal to the average magnetic field. As a result there can be considerable motion of the particles normal to the average field. Now, if the particles were to stick strictly to the meandering field lines, they would still not experience perpendicular diffusion because, as they scatter in pitch angle, they would simply move back and forth along the same field line. What is needed in addition to following the meandering of the field lines is a finite probability of scattering to another field line, which then meanders independently of the first. The net motion can result in an enhanced perpendicular diffusion.

For purposes of illustration, consider the simplest case, where the fluctuating field is assumed to have only variations of the field component which is transverse to the average magnetic field B_0, taken to be in the z direction, and which varies spatially in the direction along B_0. An approximate expression for the net motion of a particle normal to the magnetic field may be written in terms of the power spectrum of the transverse fluctuations in the magnetic field $P_\perp(k_z)$ as a function of wave number k_z along the direction of B_0. One obtains (*e.g.*, Jokipii, 1971)

$$\kappa_\perp \approx \frac{wP_\perp(k_z=0)}{B_0^2}, \tag{19}$$

which, in general, gives a much larger $\kappa_\perp/\kappa_\parallel$ than equation (18). This result is quite approximate and crude but still captures the effect of the field line meandering in an analytically tractable expression.

More recent work (for a review, see, *e.g.*, Giacalone, 1998, also, Giacalone and Jokipii, 1999) adds to the above discussion by considering direct numerical simulation of the particle motions. In all, the results confirm the conclusion that the field-line mixing is a major contributor to the perpendicular diffusion. In general, the value of $\kappa_\perp/\kappa_\parallel$ is somewhat smaller than that derived from equation (19) but still considerably larger than that given in equation (18). The computed values agree in general magnitude with those used for the past decade or so in the large-scale modelling of galactic cosmic rays (see, *e.g.*, Potgieter, 1998). It seems likely, therefore, that the magnitude of the ratio $\kappa_\perp/\kappa_\parallel$ is significantly larger than that implied by equation (18).

4.5. Relations between CIR-generated energetic particles and CIR plasma and field structures

CIRs are prolific sources of energetic ions, as described elsewhere in this issue. Their forward and reverse shocks can accelerate solar wind suprathermal ions and interstellar pickup ions from keV to MeV energies. Transport processes associated with CIRs then distribute the accelerated ions in a characteristic way in space. The purpose of this subsection is to summarize attempts to relate this observed characteristic distribution of CIR-generated energetic ions with specific CIR features and transport processes. The data used in these attempts come mainly from Pioneers 10 and 11 and Ulysses during times when CIRs were dominant solar wind features. For the Pioneers, this was in 1974, the declining phase of Solar Cycle 20, when two giant solar wind streams and associated CIRs persisted for more than a year. The Pioneers were then in the ecliptic plane in the range of 4 to 5 AU from the Sun. For Ulysses, the time of optimum observations was during the corresponding phase of Solar Cycle 22, when the numbered series of streams addressed in previous sections was encountered near 5 AU at ~30°S heliographic latitude (Bame *et al.*, 1993).

CIRs are organized spatially around stream interfaces, which, as argued below, appear to play a central role in the organization of energetic particles. As discussed in Sect. 2.1, a stream interface is a product of global dynamics and solar origins. It resides in a high-pressure front where solar rotation forces hot, tenuous, fast streams to plow into cool, dense, slow streams. It shows up in solar wind data as an increase in specific entropy. Because the increase is set by a large difference in the coronal temperatures and densities of fast and slow streams, this state persists along the full radial extent of the interface (at least out to 5 AU, where it was documented with Pioneer and Ulysses data) despite a known increase in entropy with distance that occurs throughout both streams (Siscoe and Intriligator, 1993).

A CIR's forward and reverse shocks mark its radial and azimuthal boundaries at distances beyond about 2 AU, which, as Fig. 1 indicates, is about where they first appear as the solar wind moves out from the Sun. Their points of formation stand off from the stream interface by a distance, measured in corotation time, of roughly half a day. This aspect of CIR geometry is important to the subsequent discussion. Numerical MHD simulations show that the starting points of the shocks stand off from the stream interface by a corotation time of at least 12 hours (Pizzo, 1989; Hu, 1993). We note for later reference that the role of the shocks is to deflect the flow entering the CIR from either side to be more parallel to the stream interface in the corotating reference frame. (Fig. 1 tries to show this.) Since IMF lines parallel flow lines in the corotating frame, this means that where field lines intersect a bounding shock in either stream, the lines are deflected to have nearly the same corotational spiral as the stream interface. As a corollary, field lines from the sun that go through the formation points of the shocks will maintain a nearly constant corotation distance from the stream interface of about half a day or more. Thus, on either side of the stream interface there is a layer about half a corotation day thick within which IMF lines pass through neither shock. In Fig. 1 these are labeled the leading unshocked layer (LUL) and the trailing unshocked layer (TUL).

The two border-defining CIR shocks generate a pair of corotating energetic ion populations (CEIPs). The forward shock generates the leading CEIP, and the reverse shock generates the trailing CEIP. The peaks of the CEIPs may or may not coincide with the shocks. The trailing CEIP is usually more pronounced than the leading CEIP. Between the two CEIPs is a valley of low flux having a repeatable

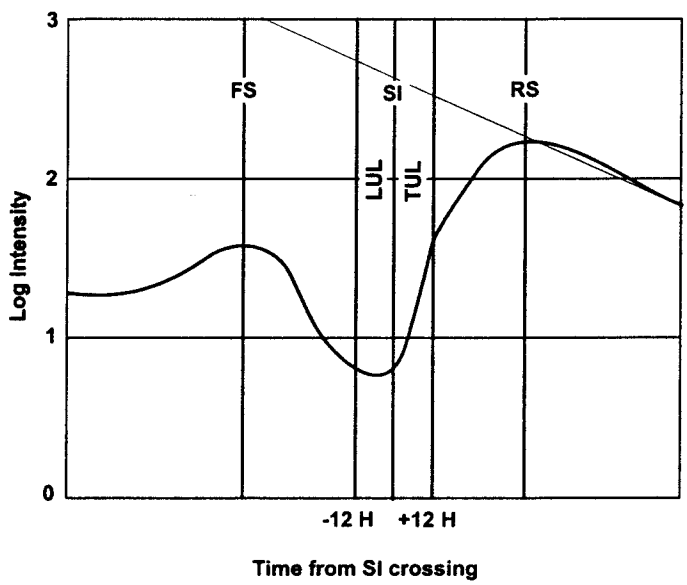

Figure 10. Idealized profile of corotating energetic ion population intensities associated with CIRs. Vertical lines mark systematic alignments between CEIP and CIR features.

form that is asymmetric in a way that is not simply a reflection of the difference in the relative peak intensities of the two CEIPs.

Fig. 10 shows a sketch of an idealized combined CIR-CEIP geometry as it might be synthesized after examining many actual (*i.e.*, non-ideal) time histories of ions with energies around 1 MeV. The figure's prominent features are the CEIP profile's two peaks and intervening valley (Barnes and Simpson, 1976; McDonald *et al.*, 1976; Pesses *et al.*, 1979). The forward and reverse shocks are near the CEIP peaks. The leading peak is weaker and briefer. The intervening valley can drop below the pre-CIR ambient intensity, as shown here, but sometimes it bottoms out above it. The factor of 20 vertical range of the CEIP profile is representative, but it can exceed 100. Defining the shape of the valley are its leading wall, its trailing wall, and the floor in between. The steeper, trailing wall lies within the trailing unshocked layer. This wall's precipitous decline halts where it hits the stream interface (Intriligator and Siscoe, 1994). (As an aside, we note that in the Pioneer data at the one-hour resolution used to analyze CEIP profiles, the stream interface and the heliospheric current sheet usually coincided. In one instance, however, the HCS preceded the SI by nearly six hours. Then it was clear that it was the SI, not the HCS, that stopped the wall.) Whereas the steepest part of the CEIP profile lies in the trailing unshocked layer, its shallowest and deepest part, the valley floor, lies in the leading unshocked layer. The leading wall joins smoothly onto the leading CEIP. In the case of the trailing wall, however, there are indications (not always present) of a break in the slope about where it exits the TUL. Such a break is suggested in the figure.

Fig. 11 shows superpositions of CEIP profiles measured by the Pioneers (upper panel) and Ulysses (lower panel) from Intriligator and Siscoe (1994) and Intriligator *et al.* (1995). The profiles are best in the Pioneer data, which served, therefore, as the models for the idealized profile of Fig. 10. The Ulysses data were taken at higher latitudes, where forward shock signatures are weaker relative to reverse shock signatures (Gosling *et al.*, 1993b). The figure shows how well individual cases conform to our idealization of them as well as how much they deviate from it. Aside from the obvious CEIP-shock association, perhaps the CEIP-CIR alignment most clearly demonstrated in these data is that between the stream interface and the foot of the valley's trailing wall. This alignment holds for all Pioneer 10, Pioneer 11, and Ulysses cases. By contrast, the widths of the leading and trailing unshocked layers are only approximately known. So, while the figure suggests that the valley floor fits inside the LUL, this suggestion is not actually established by data. A similar caveat applies to fitting the steepest part of the CEIP profile inside the TUL. We note that for Ulysses CIR 9, discussed in Sect. 4.2, the ion, especially w1, intensity profiles in Fig. 9 are consistent with the Pioneer and Ulysses CEIP intensity profiles in Fig. 11 and with the CIR geometry in Fig. 1 when modified for a case of three crossings of a wavy stream interface, appropriate to CIR 9 (Wimmer-Schweingruber *et al.*, 1997).

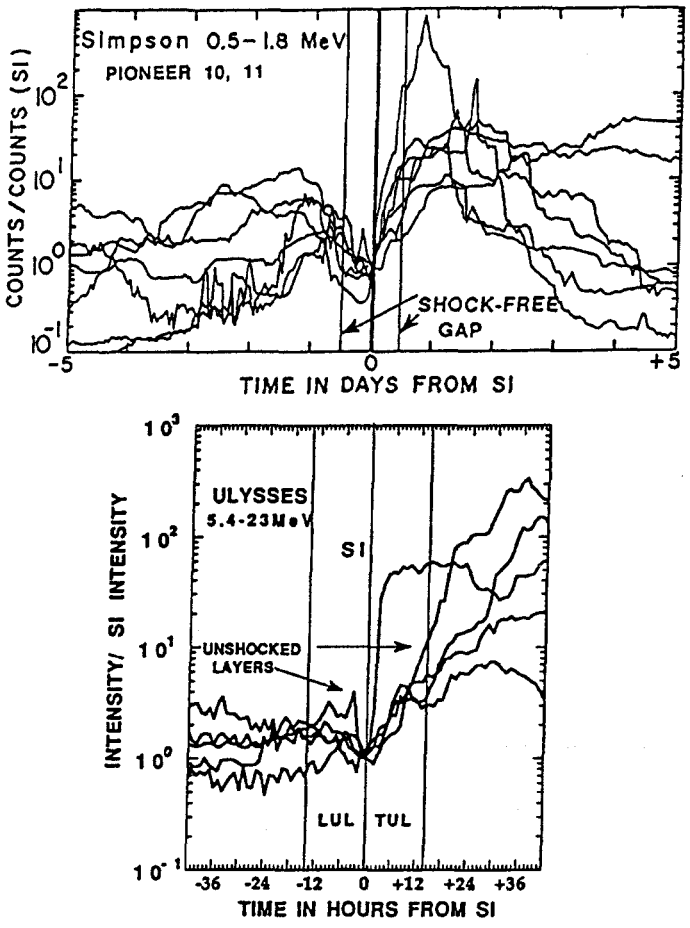

Figure 11. Superposition of CEIP intensity profiles for seven CIR encounters by Pioneer 10 or Pioneer 11 (upper panel, from Intriligator and Siscoe, 1994) and five by Ulysses (lower panel, from Intriligator *et al.*, 1995). Each profile is normalized to its value at the stream interface. The space between the two lines centered on the stream interface approximates the shock-free gap (the LUL and TUL in Fig. 10).

Consider next energetic ion transport in CIRs. (The aspect of energetic ion production at CIR shocks is considered elsewhere in this issue.) The relevant transport principle is simply that ions usually spread away from a source much faster along magnetic field lines than across them. The extreme version of this principle is that ions spread only along field lines and not across them. Applying this limit to the shocks as ion sources would give a pair of CEIPs separated by a deep valley whose flat floor would extend across both the leading and trailing unshocked layers. The stream interface would not be marked in the energetic ions. This scenario seems to get the leading half of the picture right; the valley floor in the LUL is flat and deepest, which could be interpreted to mean that it is cut off from the source of

ions. But the scenario fails in the TUL. The trailing CEIP that lies in the TUL implies cross-field transport.

Intriligator and Siscoe (1995) have quantitatively treated the problem of populating the TUL by cross-field transport from the ion-popula-ted region that is magnetically connected to the reverse-shock ion source. Cross-field diffusion driven by scattering that causes a random walk of the ions' gyrocenters is much too slow. But so-called stochastic diffusion, in which ions follow field lines which themselves randomly wander across the average field direction (Jokipii, 1966), is fast enough (see Sects. 4.4 and 4.6). The scenario follows one that Conlon (1978) had developed to explain the dispersion of Jovian electrons throughout interplanetary space. To account for the presence of Jovian electrons far from field lines that, in an average Parker-spiral sense, connect to Jupiter's magnetosphere, he needed the efficient "cross-field" transport that only stochastic diffusion can provide. But he also found that CIRs were strongly shielded from Jovian electrons, from which he inferred that cross-field transport in CIRs was reduced by two to three orders of magnitude compared to that in the ambient solar wind. Intriligator and Siscoe found that the same conclusion applies to the cross-field transport of energetic ions generated by CIR shocks. Cross-field transport by stochastic diffusion at a rate that applies to the ambient solar wind would fill the TUL essentially to the level at the source. That is, there would be no valley. Following Conlon's lead, they argued that cross-field transport by stochastic diffusion in CIRs should be slower than in the free solar wind by the square of the CIR compression ratio for the field, which reduces the rate by about two orders of magnitude. A reduction of this much allows intensity gradients as steep as observed in the TUL. It takes a balance between fast stochastic diffusion and compressional retardation to populate the TUL with neither too many nor too few ions compared to observations. We are left then with two puzzles: Why does stochastic diffusion across the TUL stop at the stream interface? And why does not such diffusion from the forward shock similarly populate the LUL?

The first puzzle seems to have a simple and satisfactory solution. The stream interface presumably is a tangential discontinuity (see Sect. 2.1), and stochastic diffusion does not operate across tangential discontinuities. Stochastic diffusion operates only over regions accessible to wandering field lines. By their nature, tangential discontinuities do not allow field lines to wander across them. Thus, the stream interface stops energetic ions generated at the reverse shock from moving into the preceding part of the CIR. This idea is explored further in the next section.

Why does the forward shock not populate the LUL like the reverse shock populates the TUL? An answer to this second puzzle along the line that energetic ion production at the forward shock is usually weaker seems inadequate. In some cases, production at the forward shock is strong enough to produce a steep wall leading into the valley; but it does not eliminate the valley floor. We suspect that the answer to this question will involve a more complete CIR model than we have considered. Possibly there is a hidden tangential discontinuity (separating domains

of quasi-parallel field lines whose solar footprints are spatially apart) between the valley floor and the forward shock, which prevents shock-generated ions from stochastically diffusing into the floor.

4.6. Suppression of Perpendicular Diffusion Near Stream Interfaces

Observations of the energetic particles associated with CIRs provide a valuable probe of the magnetic structure and cosmic-ray transport coefficients both in the CIR and throughout the heliosphere. As discussed in the preceding section, of particular interest is the rate of diffusion across the average magnetic field. Recent observations of CIR-associated energetic ions show that the diffusion of $\sim$ 100 keV-1 MeV ions across the average magnetic field is remarkably large, being in some cases larger than the parallel diffusion (Dwyer *et al.*, 1997). Here we consider further how such perpendicular diffusion might be suppressed.

Intriligator and Siscoe (1994; 1995) considered the variation in particle intensity across a CIR, addressing the question of the particle transport responsible for setting up the observed distribution. The intensity is generally highest at the reverse shock, for reasons which are not yet fully understood. As a function of distance downstream of the reverse shock in the shocked plasma, the energetic particle intensity remains high and, in some cases, roughly constant until the vicinity of the current sheet, which is close to the stream interface in the Pioneer data. At this point, the intensity drops suddenly to a much smaller value. Intriligator and Siscoe (1995) note that the most straightforward interpretation of this behaviour is that the cross-field diffusion changes abruptly to a much smaller value in this region.

An interesting question posed in the preceding section is: What may cause the observed significant decrease in the transport or diffusion across the magnetic field near the stream interface? As pointed out by Intriligator and Siscoe (1995), it is likely that the relatively large cross-field transport is the result of random walk, or braiding of the magnetic field lines. This concept is discussed more fully in Sect. 4.4. The question may then be reduced to: What process can significantly reduce or eliminate the random walk in this region of space?

One simple model which can accomplish this is shown in Fig. 12, which illustrates schematically the streamer belt at the sun. As discussed by Jokipii and Parker (1968) (see, also, Fisk and Jokipii, 1999), random walk or braiding of magnetic field lines may be produced near the Sun by convection and reconnection of field lines in association with supergranulation motions. These are illustrated in Fig. 12 by the arrows at the solar surface. On either side of the streamer belt, the fast solar wind flows outward, carrying with it the photospheric magnetic field. Clearly, the braiding of the field lines occurring at the surface is embedded in this flow. This is consistent with observations of the magnetic field observed at Ulysses (Jokipii *et al.*, 1995). But it is also apparent that the random walk occurring in the region of the streamer belt is not convected out into the solar wind. Field lines that meet at the

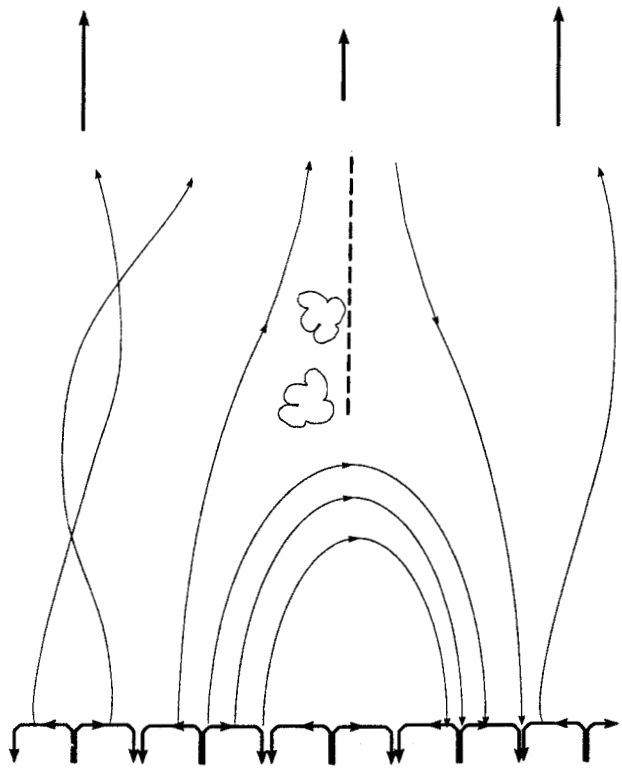

Figure 12. Schematic illustration of the suppression of field-line random walk or braiding in the vicinity of the streamer belt. The supergranular motions at the solar surface are shown near the bottom, and the closed magnetic fields of the streamer belt are illustrated by the arches. The clouds indicate the slow wind, and the dashed line is the heliospheric current sheet.

dashed line, representing the interface/HCS, cannot braid at the surface because their origins are not adjacent there. Further, as argued in the preceding section, they cannot braid across the dashed line in interplanetary space, since presumably it is a tangential discontinuity. The result should be a considerable lessening of the perpendicular diffusion of the charged particles in the region of space near the stream interface/HCS.

What Fig. 12 neglects is the distinction made in the previous section that when the interface and HCS are clearly separated in the hourly averaged data, it is at the interface, not at the HCS, where the particle intensity changes. If the interface is the field line to the right of the dashed line separating slow from fast flow, then the figure does not illustrate why field lines cannot braid at the surface across the interface. Nevertheless, some variant of this simple picture, for example, one with multiple closed field line regions in the slow wind source region, may account for the pattern identified by Intriligator and Siscoe (1994) and Intriligator *et al.* (1995).

4.7. Evolution with Heliocentric Distance

The mid-1970's solar minimum period provided a unique opportunity to study the evolution of CIRs with heliocentric distance. Observations were available from the Helios 1 and 2 spacecraft at 0.3-1 AU, near-Earth spacecraft, and Pioneer 10 and 11 at several AU. Fig. 13 shows observations of energetic particles ($\sim$ 3 MeV protons and cosmic rays), plasma, and the magnetic field (in HSE coordinates) at Earth and Pioneers 10 and 11 for a representative CIR in April 1974. The CIR was formed ahead of a high-speed stream which had sunward-directed magnetic fields.

At 1 AU (left panel), the plasma density and magnetic field enhancements associated with the developing CIR encompass the stream interface (I) but have poorly defined boundaries. There are features suggestive of developing reverse shocks, labeled "R?," on April 19 and 20. The heliospheric current sheet was encountered on April 16, $\sim$2 days prior to the interface crossing. To give a general indication of the magnetic field turbulence levels, the bottom panel shows the sum of the squares of the field component variances during 1-hour averaging periods. Note that turbulence levels increase around and following the interface in the region where the solar wind speed is increasing. The energetic particle data show an enhancement

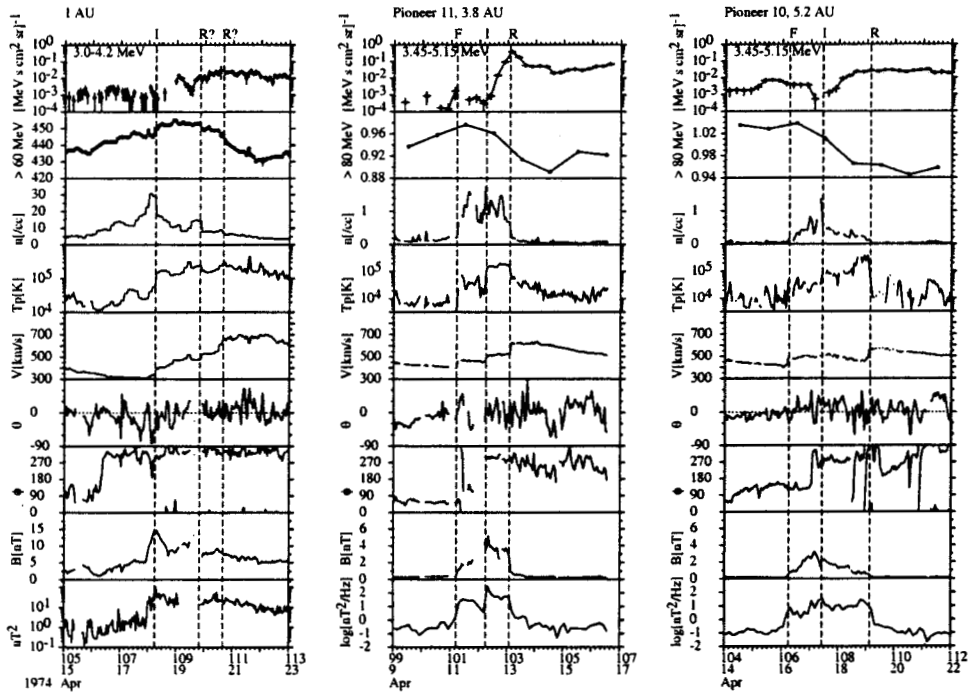

Figure 13. Energetic particle, solar wind plasma, and magnetic field observations of a CIR at 1 AU (left), Pioneer 11 (3.8 AU; centre), and Pioneer 10 (5.2 AU; right). Vertical lines indicate forward (F) and reverse (R) shocks, and the stream interface (I). The magnetic field azimuthal angle ϕ is given in HSE coordinates such that 0° corresponds to a radially-sunward directed field.

of a-few-MeV protons in the high-speed stream. A depression in the cosmic ray density (indicated by the counting rate of the anticoincidence guard of the IMP 8 GME instrument, which detects >60 MeV particles) commenced near the trailing edge of the interaction region and extended into the high-speed stream. The data illustrate the general conclusion of Richardson *et al.* (1996) that, at $\leq$1 AU, CIR-associated cosmic ray depressions occur within the high-speed flow and tend to be anticorrelated with the solar wind speed. Such depressions also appear to be less closely related to magnetic field enhancements associated with CIRs than would be expected based on the often-used assumption (see references in Wibberenz *et al.*, 1998) that particle scattering is proportional to the magnetic field strength.

At Pioneer 11 (centre panel; 3.8 AU, 5°N), forward (F) and reverse (R) shocks bound the CIR. The abrupt increases in the solar wind speed and proton temperature midway between the shocks indicate the stream interface. The heliospheric current sheet has been swept up into the CIR and is crossed (during a data gap) just ahead of the interface (a counterexample to the fixed interface-HCS relationship discussed in Sect. 4.5). The MeV proton intensity around the reverse shock is higher than at the forward shock, as is typical for near-ecliptic CIRs at several AU (*e.g.*, Barnes and Simpson, 1976; Desai *et al.*, 1998). The cosmic ray density (24-hour averages of the > 80 MeV proton counting rate from the University of Iowa instrument) shows a depression inside the high-speed stream. This commences in the vicinity of the CIR, but the low counting rate and consequent time-averaging does not allow the associated solar wind structure to be identified precisely. Magnetic field fluctuations are represented in the bottom panel by the power at wavenumbers of $1.6 - 3.3 \times 10^{-5}$ km^{-1} (resonant with a-few-MeV protons) obtained from an Elsässer variable analysis of 1-min averaged data (Horbury and Schmidt, 1999). (Such data are not available at 1 AU during the period in Fig. 13 so a similar analysis cannot be made.) Enhanced turbulence levels are evident in the CIR, in particular following the stream interface. Similar features can be identified at Pioneer 10 (right-hand panel; 5.2 AU, 7°N). The few-MeV proton enhancement at the reverse shock, however, was smaller at Pioneer 10 than at Pioneer 11, whereas that at the forward shock was more intense. This suggests that the particle acceleration efficiency at each shock had a different dependence on heliocentric distance. For the reverse shock, the acceleration efficiency was apparently highest between 3.8 and 5.2 AU. Van Hollebeke *et al.* (1978) also concluded that particle acceleration at CIRs is most efficient at several AU from the Sun and decreases at larger distances. It is likely that the particle enhancement observed in the high-speed stream at 1 AU consisted of sunward-streaming particles accelerated at the CIR reverse shock beyond 1 AU. The 1 AU observations indicate that these particles extended onto field lines within the CIR which are not connected to the CIR reverse shock, providing evidence for cross-field diffusion within the CIR beyond 1 AU.

Fig. 14 shows the evolution of the high-speed stream structure and CIRs at 0.4 to 4.5 AU during a period of about one solar rotation in early 1975. The intervals

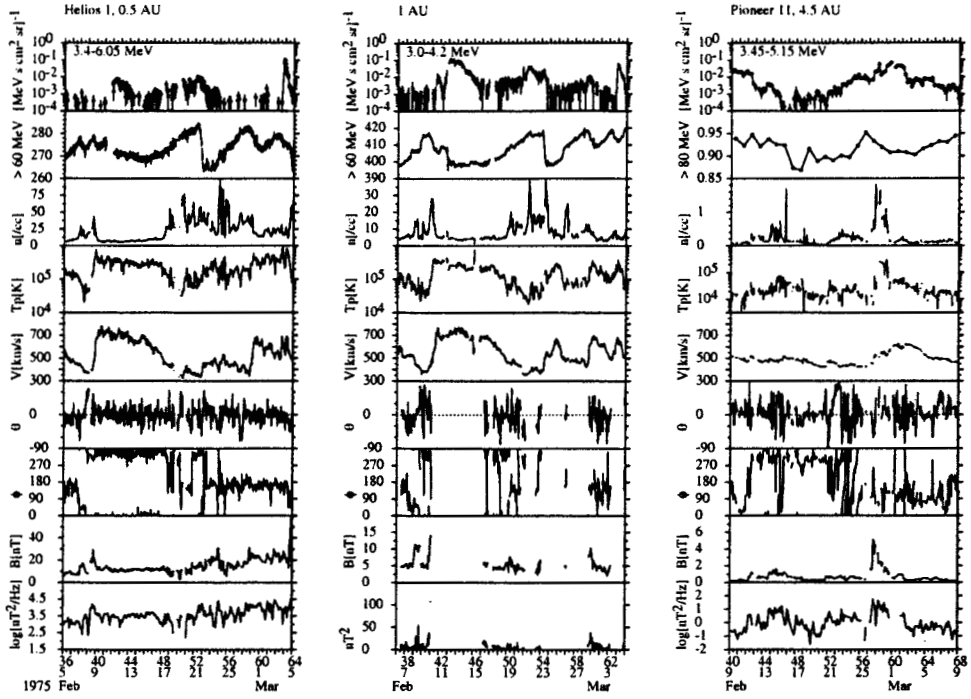

Figure 14. Evolution of two high-speed streams and the associated CIRs between ~0.5 AU (Helios 1; left), 1 AU (centre), and 4.5 AU (Pioneer 11; right).

shown have been chosen to allow for corotation delays between the spacecraft so that corotating structures, such as high-speed streams and magnetic field sector boundaries, lie at similar horizontal locations in each panel. At Helios 1 (left panel; 0.4-0.7 AU), the sunward magnetic sector ($\phi \sim 315°$.) includes an extended high-speed stream associated with a-few-MeV proton enhancement and cosmic ray depression (observed by the anti-coincidence guard of the University of Kiel instrument). The antisunward sector ($\phi \sim 135°$) includes more structured high-speed flows associated with distinct cosmic ray depressions. Similar features are evident at 1 AU (centre panel) but with small-scale differences which may arise, for example, from the different spacecraft heliolatitudes. At Pioneer 11 (right panel; 4.5 AU, 8.5°N), the high-speed streams are less pronounced than at $\leq$ 1 AU, as is typically found (*e.g.*, Burlaga *et al.*, 1983). Similar features, however, can be identified in the plasma density, magnetic field and cosmic rays, showing that the underlying structures evident at $\leq$1 AU are still present. The most prominent stream, CIR (in the magnetic field data), and MeV particle enhancements at Pioneer 11 are in the antisunward sector, in contrast to $\leq$1 AU, where these features are more pronounced in the sunward sector. The low, few-MeV particle intensities in the sunward sector at Pioneer 11 suggest that the particles observed in this sector at $\leq$1 AU must have been accelerated well within 4.5 AU. The reduction in the

particle acceleration efficiency may have been related to the erosion of the related stream between 1 AU and Pioneer 11. There are cosmic ray depressions in the corotating streams at Pioneer 11. Observations at Pioneer 10 (6.8 AU, 8.5°N) are intermittent and not shown here but are generally similar to those at Pioneer 11. These observations illustrate how CIRs may evolve differently with heliocentric distance as the interaction of multiple streams reduces azimuthal solar wind speed variations in the outer heliosphere.

5. Conclusions

The basic morphology of CIR plasma and field features is well understood, but complexities regarding the relative positions of features, variability of feature signatures, multiples of features, and transient features are topics of current studies. Rather than simply resolving details, these studies may yield refreshing new views of global heliospheric structure and dynamics. Patterns of magnetic fluctuations and energetic particles relative to the basic plasma and field features are reasonably well understood in a statistical sense, but they raise a number of questions currently under investigation regarding particle transport, particle acceleration, and the interaction of fluctuations with shocks and structures. These studies are expected to yield a greater understanding of the dependence of energetic particle propagation on magnetic field fluctuations and structures within and around CIRs, and hence the energetic particle population throughout the heliosphere.

Acknowledgements

We are grateful to H. Kunow for conceiving of and organizing the workshop series that resulted in this volume and to the International Space Science Institute, Bern, for sponsoring the final workshop and book publication. Research for this paper was supported in part by NASA under grant NAG5-6658 (NUC), grant NAG5-1476 (MAL), grant NGC 5-180 (IGR), and JPL Voyager contract 959203 to MIT (AJL), by NSF under grant ATM96-333366 (MAL), by Carmel Research Center (DSI, GLS), and by the Schweizerischer Nationalfonds (RFWS). Portions of the research were carried out at the Jet Propulsion Laboratory, Calif. Inst. Tech., under contract with NASA, and at Los Alamos National Laboratory under the auspices of the U. S. Department of Energy, with support from NASA.

References

Asbridge, J. R., Bame, S. J. and Feldman, W. C.: 1976, 'Helium and Hydrogen Velocity Differences in the Solar Wind', *J. Geophys. Res.* **81**, 2,719–2,727.

Balogh, A., Bothmer, V., Crooker, N. U., Forsyth, R. J., Gloeckler, G., Hewish, A., Hilchenbach, M., Kallenbach, R., Klecker, B., Linker, J. A., Lucek, E., Mann, G., Marsch, E., Posner, A., Schmidt, J. M., Scholer, M., Wang, Y.-M., Wimmer-Schweingruber, R. F., Aellig, M. R., Bochsler, P., and Mikić, Z.: 1999, 'The Solar Origin of Corotating Interaction Regions', *Space Sci. Rev.*, this volume.

Bame, S. J., Asbridge, J. R., Feldman, W. C., and Gosling, J. T.: 1977, 'Evidence for a Structure-Free States at High Solar Wind Speeds', *J. Geophys. Res.* **82**, 1,487–1,492.

Bame, S. J., Goldstein, B. E., Gosling, J. T., Harvey, J. W., McComas, D. J., Neugebauer, M., and Phillips, J. L.: 1993, 'Ulysses Observations of a Recurrent High Speed Solar Wind Stream and the Heliomagnetic Streamer Belt', *Geophys. Res. Lett.* **20**, 2323–2326.

Barnes, C. W., and Simpson, J. A.: 1976, 'Evidence for Interplanetary Acceleration of Nucleons in Corotating Interaction Regions', *Astrophys. J. Lett.* **210**, L91–L96.

Bavassano B., Woo, R., and Bruno, R.: 1997, 'Heliospheric Plasma Sheet and Coronal Streamers', *Geophys. Res. Lett.* **24**, 1655–1658.

Belcher, J. W. and Davis Jr., L.: 1971, 'Large-Amplitude Alfvén Waves in the Interplanetary Medium, 2', *J. Geophys. Res.* **76**, 3534–3563.

Borrini, G., Wilcox, J. M., Gosling, J. T., Bame, S. J. and Feldman, W. C.: 1981, 'Solar Wind Helium and Hydrogen Structure near the Heliospheric Current Sheet: A Signal of Coronal Streamers at 1 AU', *J. Geophys. Res.* **86**, 4,565–4,573.

Burlaga, L. F.: 1974, 'Interplanetary Stream Interfaces', *J. Geophys. Res.* **79**, 3,717–3,725.

Burlaga, L. F.: 1988, 'Interaction Regions in the Distant Solar Wind', *in* V. J. Pizzo, T. E. Holzer, and D. G. Sime (eds), *Proceedings of the Sixth International Solar Wind Conference, Tech Note NCARR/TN-306*, Natl. Cent. for Atmos. Res., Estes Park, Colo., pp. 547–562.

Burlaga, L. F.: 1991, 'Magnetic Clouds', *in* R. Schwenn and E. Marsch (eds.), *Physics of the Inner Heliosphere 2*, Springer-Verlag, Berlin, pp. 1–22.

Burlaga, L. F., Schwenn, R., and Rosenbauer, H.: 1983, 'Dynamical Evolution of Interplanetary Magnetic Fields and Flows between 0.3 AU and 8.5 AU: Entrainment', *Geophys. Res. Lett.* **10**, 413–416.

Burlaga, L. F., Pizzo, V. J., Lazarus, A. J., and Gazis, P. R.: 1985, 'Stream Dynamics between 1 AU and 2 AU: A Comparison of Observations and Theory', *J. Geophys. Res.* **90**, 7,377–7,388.

Burton, M. E., Neugebauer, M., Crooker, N. U., von Steiger, R., and Smith, E. J.: 1998, 'Identification of Trailing Edge Solar Wind Stream Interfaces: A Comparison of Ulysses Plasma and Composition Measurements', *J. Geophys. Res., in press.*

Colburn, D. S. and Sonett, C. P.: 1966, 'Discontinuities in the Solar Wind', *Space Sci. Rev.* **5**, 439.

Conlon, T. F.: 1978, 'The Interplanetary Modulation and Transport of Jovian Electrons', *J. Geophys. Res.* **83**, 541–552.

Crooker, N. U. and Intriligator, D. S.: 1996, 'A Magnetic Cloud at Pioneers 10 and 11: Relation to Heliospheric Current Sheet, Stream Interface, and Energetic Ions', *in* D. Winterhalter, J. Gosling, S. Habbal, W. Kurth and M. Neugebauer (eds), *Solar Wind Eight*, Amer. Inst. Phys., New York, pp. 442–444.

Crooker, N. U., Burton, M. E., Smith, E. J., Phillips, J. L., and Balogh, A.: 1996a, 'Heliospheric Plasma Sheets as Small-Scale Transients', *J. Geophys. Res.* **101**, 2,467–2,474.

Crooker, N. U., Burton, M. E., Siscoe, G. L., Kahler, S. W., Gosling, J. T., and Smith, E. J.: 1996b, 'Solar Wind Streamer Belt Structure', *J. Geophys. Res.* **101**, 24,331–24,341.

Crooker, N. U., Gosling, J. T., and Kahler, S. W.: 1998, 'Magnetic Clouds at Sector Boundaries', *J. Geophys. Res.* **103**, 301–306.

Crooker, N. U., Shodhan, S., Forsyth, R. J., Burton, M. E., Gosling, J. T., Fitzenreiter, R. J., and Lepping, R. P.: 1999, 'Transient Aspects of Stream Interface Signatures', *in* S. Habbal *et al.* (eds), *Solar Wind Nine*, Amer. Inst. Phys., New York, in press.

Desai, M. I., Marsden, R. G., Sanderson, T. R., Balogh, A., Forsyth, R. J., and Gosling, J. T.: 1998, 'Particle Acceleration at Corotating Interaction Regions in the Three-Dimensional Heliosphere', *J. Geophys. Res.* **103**, 2,003–2,014.

Dwyer, J. R., Mason, G. M., Mazur, J. E., Jokipii, J. R., von Rosenvinge, T. T., and Lepping, R. P.: 1997, 'Perpendicular Transport of Low-Energy Corotating Interaction Region-Associated Nuclei', *Ap. J. Lett.* **490**, L115–L118.

Fisk, L. T. and Jokipii, J. R.: 1999, 'Mechanisms for Latitudinal Transport of Energetic Particles in the Heliosphere', *Space Sci. Rev.*, this volume.

Forsyth, R. J., Balogh, A., Smith, E. J., and Gosling, J. T.: 1997, 'Ulysses Observations of the Northward Extension of the Heliospheric Current Sheet', *Geophys. Res. Lett.* **24**, 3101–3104.

Forsyth, R. J. and Marsch, E.: 1999, 'Solar Origin and Conditions and the Development of Stream Interfaces', *Space Sci. Rev.*, this volume.

Gazis, P. R., McDonald, F. B. *et al.*: 1999, 'Co-rotating Interaction Regions in the Outer Heliosphere', *Space Sci. Rev.*, this volume.

Geiss, J., Gloeckler, G., and von Steiger, R.: 1995, 'Origin of the Solar Wind from Composition Measurements', *Space Sci. Rev.* **72**, 49–60.

Giacalone, J.: 1998, 'Cosmic-Ray Transport Coefficients', *Space Sci. Rev.* **83**, 351–363.

Giacalone, J., and Jokipii, J. R., 1999: 'Transport of Cosmic Rays Across the Average Magnetic Field', *Astrophys. J.* in press.

Gonzalez-Esparza, J. A., and Smith, E. J.: 1997, 'Three-Dimensional Nature of Interaction Regions: Pioneer, Voyager, and Ulysses Solar Cycle Variations from 1 to 5 AU', *J. Geophys. Res.* **102**, 9,781–9,792.

Gosling, J. T. and Pizzo, V. J.: 1999, 'Formation and Evolution of CIRs and their 3-D Structure', *Space Sci. Rev.*, this volume.

Gosling, J. T., Asbridge, J. R., Bame, S. J. and Feldman, W. C.: 1978, 'Solar Wind Stream Interfaces', *J. Geophys. Res.* **83**, 1,401–1,412.

Gosling, J. T., Borrini, G., Asbridge, J. R., Bame, S. J., Feldman, W. C. and Hansen, R. F.: 1981, 'Coronal Streamers in the Solar Wind at 1 AU', *J. Geophys. Res.* **86**, 5,438–5,448.

Gosling, J. T.: 1990, 'Coronal Mass Ejections and Magnetic Flux Ropes in Interplanetary Space', *in* C. T. Russell, E. R. Priest, and L. C. Lee (eds.), *Physics of Magnetic Flux Ropes*, Geophys. Monogr. Ser., Vol. 58, AGU, Washington, D.C., pp. 343–364.

Gosling, J. T., Bame, S. J., Feldman, W. C., McComas, D. J., Phillips, J. L., and Goldstein, B. E.: 1993a, 'Counterstreaming Suprathermal Electron Events Upstream of Corotating Shocks in the Solar Wind Beyond ~2 AU: Ulysses', *Geophys. Res. Lett.* **20**, 2335–2338.

Gosling, J. T, Bame, S. J., McComas, D. J., Phillips, J. L., Pizzo, V. J., Goldstein, B. E., and Neugebauer, M.: 1993b, 'Latitudinal Variation of Solar Wind Corotating Interaction Regions: Ulysses', *Geophys. Res. Lett.* **20**, 2789–2792.

Hoeksema, J. T.: 1995, 'The Large-Scale Structure of the Heliospheric Current Sheet during the Ulysses Epoch', *Space Sci. Rev.* **72**, 137–148.

Horbury, T. S. and Schmidt, J.: 1999, 'Development and Effects of Turbulence in Connection with CIRs', *Space Sci. Rev.*, this volume.

Hu, Y. Q.: 1993, 'Evolution of Corotating Stream Structures in the Heliospheric Equatorial Plane', *J. Geophys. Res.* **98**, 13,201–13,214.

Hundhausen, A. J.: 1973, 'Nonlinear Model of High-Speed Solar Wind Streams', *J. Geophys. Res.* **78**, 1,528–1,542.

Hundhausen, A. J. and Gosling, J. T.: 1976, 'Solar Wind Structure at Large Heliocentric Distances: An Interpretation of Pioneer 10 Observations', *J. Geophys. Res.* **81**, 1,436–1,440.

Intriligator, D. S., and Siscoe, G. L.: 1994, 'Stream Interfaces and Energetic Ions Closer than Expected - Analyses of Pioneer 10 and Pioneer 11 Observations', *Geophys. Res. Lett.* **21**, 1117–1120.

Intriligator, D. S. and Siscoe, G. L.: 1995, 'Cross-Field Diffusion in Corotating Interaction Regions', *J. Geophys. Res.* **100**, 21,605–21,612.

Intriligator, D. S., Siscoe, G. L., Wibberenz, G., Kunow, H., and Gosling, J. T.: 1995, 'Stream Interfaces and Energetic Ions - II. Ulysses Test of Pioneer Results', *Geophys. Res. Lett.* **22**, 1173–1176.

Jokipii, J. R.: 1966, 'Cosmic Ray Propagation - I. Charged Particles in a Random Magnetic Field', *Astrophys. J.* **145**, 480.

Jokipii, J. R.: 1971, 'Propagation of Cosmic Rays in the Solar Wind', *Rev. Geophysics* **9**, 27–87.

Jokipii, J. R. and Parker E. N.: 1969, 'Random Walk of Magnetic Lines of Force in Astrophysics', *Phys. Rev. Lett.* **21**, 44.

Jokipii, J. R., Kóta, J., Giacalone, J., Horbury, T. S., and Smith, E. J.: 1995, 'Interpretation and Consequences of Large-Scale Magnetic Variances at High Heliographic Latitude', *Geophys. Res. Lett.* **22**, 3385–3388.

Kahler, S., Crooker, N. U., and Gosling, J. T.: 1998, 'Properties of Interplanetary Magnetic Sector Boundaries Based on Electron Heat-Flux Flow Directions', *J. Geophys. Res.* **103**, 20,603–20,612.

Kennel, C. F. and Petschek, H. E.: 1966, 'Limits on Stably Trapped Particle Fluxes', *J. Geophys. Res.* **71**, 1–28.

Kóta, J., and Jokipii, J. R.: 1983, 'Effects of Drift on the Transport of Cosmic Rays - VI. A Three-Dimensional Model Including Diffusion', *Astrophys. J.* **265**, 573–581.

Krieger, A. S., Timothy, A. F., and Roelof, E. C.: 1973, 'A Coronal Hole and its Identification as the Source of a High Velocity Solar Wind Stream', *Solar Phys.* **29**, 505–525.

Kunow, H., Lee, M. A., Fisk, L. A., Forsyth, R. J., Gosling, J. T., Heber, B., Horbury, T. S., Kóta, J., McKibben, R. B., Paizis, C., Potgieter, M. S., Roelof, E. C., Sanderson, T. R., Simnett, G. M., von Steiger, R., Tsurutani, B., and Wimmer-Schweingruber, R. F.: 1999, *Space Sci. Rev.*, this volume.

Lee, M. A.: 1999, 'An analytical theory of the morphology, flows, and compressions at corotating interaction regions in the solar wind', manuscript in preparation.

Marsch, E., Mühlhäuser, K. H., Rosenbauer, H., Schwenn, R. and Neubauer, F. M.: 1982, 'Solar Wind Helium Ions: Observations of the Helios Solar Probes between 0.3 and 1 AU', *J. Geophys. Res.* **87**, 35–51.

Mason, G. M., von Steiger, R., Decker, R. B., Desai, M. I., Dwyer, J. R., Fisk, L. A., Gloeckler, G., Gosling, J. T., Hilchenbach, M., Kallenbach, R., Keppler, E., Klecker, B., Kunow, H., Mann, G., Sanderson, T. R., Simnett, G. M., Wang, Y.-M., Wimmer-Schweingruber, R. F., Fränz, M., Mazur, J. E., Richardson, I. G.: 1999, 'Origin, injection, and acceleration of CIR particles: Observations', *Space Sci. Rev.* **this issue**.

McComas, D. J., Riley, P., Gosling, J. T., Balogh, A. and Forsyth, R.: 1998, 'Ulysses' Rapid Crossing of the Polar Coronal Hole Boundary', *J. Geophys. Res.* **103**, 1955–1967.

McDonald, F. B., Teegarden, T. J., Trainor, J. H., von Rosenvinge, T. T., and Webber, W. R.: 1976, 'The Acceleration of Energetic Ions', *Astrophys. J. Lett.* **203**, L149–L154.

Neugebauer, M., Goldstein, B. E., Smith, E. J. and Feldman, W. C.: 1996, 'Ulysses Observations of Differential Alpha-Proton Streaming in the Solar Wind', *J. Geophys. Res.* **101**, 17,047–17,055.

Palmer, I. D. and Gosling, J. T.: 1978, 'Shock-Associated Energetic Proton Events at Large Heliocentric Distances', *J. Geophys. Res.* **83**, 2,037–2,046.

Pesses, M. E., Tsurutani, B. T., Van Allen, J. A., and Smith, E. J.: 1979, 'Acceleration of Energetic Protons by Interplanetary Shocks', *J. Geophys. Res.* **84**, 7,297–7,301.

Pizzo, V. J.: 1989, 'The Evolution of Corotating Stream Fronts near the Ecliptic Plane in the Inner Solar System - I. Two-Dimensional Fronts', *J. Geophys. Res.* **94**, 8,673–8,684.

Pizzo, V. J.: 1991, 'The Evolution of Corotating Stream Fronts near the Ecliptic Plane in the Inner Solar System - II. Three-Dimensional Tilted-Dipole Fronts', *J. Geophys. Res.* **96**, 5,405–5,420.

Pizzo, V. J.: 1994, 'Global, Quasi-Steady Dynamics of the Distant Solar Wind - II. Deformation of the Heliospheric Current Sheet', *J. Geophys. Res.* **99**, 4,185–4,191.

Potgieter, M. S.: 1998, 'The Modulation Of Galactic Cosmic Rays In The Heliosphere: Theory And Models', *Space Sci. Rev.* **83**, 147–158.

Richardson, I. G., Wibberenz, G., and Cane, H. V.: 1996, 'The Relationship between Recurring Cosmic Ray Depressions and Corotating Solar Wind Streams at $\leq$ 1 AU: IMP 8 and Helios 1 and 2 Anticoincidence Guard Rate Observations', *J. Geophys. Res.* **101**, 13,483–13,496.

Scholer, M., Mann, G., Chalov, S., Desai, M. I., Fisk, L. A., Jokipii, J. R., Kallenbach, R., Keppler, E., Kóta, J., Kunow, H., Lee, M. A., Sanderson, T. R., and Simnett, G. M.: 1999, 'Origin, injection, and acceleration of CIR particles: Theory', *Space Sci. Rev.*, this volume.

Simnett, G. M. and Roelof, E. C.: 1995, 'Reverse Shock Acceleration of Electrons and Protons at Mid-Heliolatitudes from 5.3–3.8 AU', *Space Sci. Rev.* **72**, 303–308.

Siscoe, G. L., Goldstein, B., and Lazarus, A. J.: 1969, 'An East-West Asymmetry in the Solar Wind Velocity', *J. Geophys. Res.* **74**, 1,759–1,762.

Siscoe, G. and Intriligator, D.: 1993, 'Three Views of Two Giant Streams - Aligned Observations at 1 AU, 4.6 AU, and 5.9 AU', *Geophys. Res. Lett.* **20**, 2,267–2,270.

Smith, E. J.: 1973a, 'Identification of Interplanetary Tangential and Rotational Discontinuities', *J. Geophys. Res.* **78**, 2,054–2,063.

Smith, E. J.: 1973b, 'Observed properties of interplanetary rotational discontinuities', *J. Geophys. Res.* **78**, 2,088–2,093.

Smith, E. J. and Wolfe, J. H.: 1976, 'Observations of Interaction Regions and Corotating Shocks Between One and Five AU: Pioneers 10 and 11', *J. Geophys. Res.* **3**, 137–140.

Smith, E. J., Neugebauer, M., Balogh, A., Bame, S. J., Erdös, G., Forsyth, R. J., Goldstein, B. E., Phillips, J. L., and Tsurutani, B. T.: 1993, 'Disappearance of the Heliospheric Sector Structure at Ulysses', *Geophys. Res. Lett.* **20**, 2327–2330.

Thomas, B. T. and Smith, E. J.: 1981, 'The Structure and Dynamics of the Heliospheric Current Sheet', *J. Geophys. Res.* **86**, 11,105–11,110.

Tsurutani, B. T. and Smith, E. J.: 1979, 'Interplanetary discontinuities: Temporal varaiations and the radial gradient from 1 to 8.5 AU', *J. Geophys. Res.* **84**,

Tsurutani, B. T. and Thorne, R. M.: 1982, 'Diffusion Processes in the Magnetopause Boundary Layer', *Geophys. Res. Lett.* **9**, 1247.

Tsurutani, B. T., Ho, C. M., Arballo, J. K., Goldstein, B. E.: 1995, 'Large amplitude IMF fluctuations in corotating interaction regions: Ulysses at midlatitudes', *Geophys. Res. Lett.* **22**, 3397–3400.

Van Hollebeke, M.A.I., McDonald, F. B., and von Rosenvinge, T. T.: 1978, 'The Radial Variation of Corotating Particle Streams in the Inner and Outer Solar System', *J. Geophys. Res.* **83**, 4,723–4,731.

Wibberenz, G., Le Roux, J. A., Potgieter, M. S., and Bieber, J. W.: 1998, 'Transient Effects and Disturbed Conditions: Report of Working Group 4', *Space Sci. Rev.* **83**, 309–348.

Wimmer-Schweingruber, R. F., von Steiger, R. and Paerli, R.: 1997, 'Solar Wind Stream Interfaces in Corotating Interaction Regions: SWICS/Ulysses Results', *J. Geophys. Res.* **102**, 17,407–17,417.

Winterhalter, D., Smith, E. J., Burton, M. E., Murphy, N., and McComas, D. J.: 1994, 'The Heliospheric Plasma Sheet', *J. Geophys. Res.*, **99**, 6,667–6,680.

Address for Offprints: N. U. Crooker, Center for Space Physics, Boston University, Boston, Massachusetts, USA